Variational Multiscale Stabilization and p-adaptivity of High-Order Spectral Elements for the Convection-Diffusion Equation

S. Marras[a,**], J. F. Kelly[b], F. X. Giraldo[b,*], M. Vázquez[a]

[a] *Barcelona Supercomputing Center BSC-CNS. Barcelona, Spain*
[b] *Applied Mathematics, Naval Postgraduate School. Monterey (CA), U.S.A.*

Abstract

One major issue in the accurate solution of convection-dominated problems by means of high-order methods is the ability of the solver to maintain monotonicity. This problem is critical for spectral elements, where Gibbs oscillations may pollute the solution. However, typical filter-based stabilization techniques used with spectral elements are not monotone. In this paper, residual-based stabilization methods originally derived for finite elements are constructed and applied to high-order spectral elements. In particular, we show that the use of the Variational Multiscale (VMS) method greatly improves the solution of the transport-diffusion equation by reducing over- and under-shoots, and can be therefore considered an alternative to the limitations of filter-based schemes. We also combine these methods with discontinuity capturing schemes to suppress oscillations that may occur in proximity of boundary or internal layers. Additional improvement in the solution is also obtained when p-adaptivity is used in combination with VMS in the regions where discontinuities occur. The algorithms are assessed with the solution of classical steady and transient one- and two-dimensional problems using spectral elements up to order *16*.

Keywords: Spectral Elements; High-Order Methods; Variational Multiscale Method; Transport; Numerical Weather Prediction; p-adaptivity; Monotonic Methods

[*] fxgirald@nps.edu
[**] simone.marras@bsc.es

Report Documentation Page

Form Approved
OMB No. 0704-0188

1. REPORT DATE	2. REPORT TYPE	3. DATES COVERED
26 JUL 2011		**00-00-2011 to 00-00-2011**

4. TITLE AND SUBTITLE
Variational Multiscale Stabilization and p-adaptivity of High-Order Spectral Elements for the Convection-Diffusion Equation

5a. CONTRACT NUMBER
5b. GRANT NUMBER
5c. PROGRAM ELEMENT NUMBER

6. AUTHOR(S)

5d. PROJECT NUMBER
5e. TASK NUMBER
5f. WORK UNIT NUMBER

7. PERFORMING ORGANIZATION NAME(S) AND ADDRESS(ES)
Naval Postgraduate School,Department of Applied Mathematics,Monterey,CA,93943

8. PERFORMING ORGANIZATION REPORT NUMBER

9. SPONSORING/MONITORING AGENCY NAME(S) AND ADDRESS(ES)

10. SPONSOR/MONITOR'S ACRONYM(S)
11. SPONSOR/MONITOR'S REPORT NUMBER(S)

12. DISTRIBUTION/AVAILABILITY STATEMENT
Approved for public release; distribution unlimited

13. SUPPLEMENTARY NOTES

14. ABSTRACT

One major issue in the accurate solution of convection-dominated problems by means of high-order methods is the ability of the solver to maintain monotonicity. This problem is critical for spectral elements, where Gibbs oscillations may pollute the solution. However, typical filter-based stabilization techniques used with spectral elements are not monotone. In this paper, residual-based stabilization methods originally derived for finite elements are constructed and applied to high-order spectral elements. In particular we show that the use of the Variational Multiscale (VMS) method greatly improves the solution of the transport-diffusion equation by reducing over- and under-shoots, and can be therefore considered an alternative to the limitations of filter-based schemes. We also combine these methods with discontinuity capturing schemes to suppress oscillations that may occur in proximity of boundary or internal layers. Additional improvement in the solution is also obtained when p-adaptivity is used in combination with VMS in the regions where discontinuities occur. The algorithms are assessed with the solution of classical steady and transient one- and two-dimensional problems using spectral elements up to order 16.

15. SUBJECT TERMS

16. SECURITY CLASSIFICATION OF:			17. LIMITATION OF ABSTRACT	18. NUMBER OF PAGES	19a. NAME OF RESPONSIBLE PERSON
a. REPORT	b. ABSTRACT	c. THIS PAGE			
unclassified	**unclassified**	**unclassified**	**Same as Report (SAR)**	**45**	

1. Introduction

A large number of physical applications relies on the accurate solution of the transport-diffusion equation

$$\mathcal{L}(q) := \frac{\partial q}{\partial t} + \mathbf{u} \cdot \nabla q - \nu \Delta q = f, \tag{1}$$

where $\nu > 0$ is a diffusion coefficient, $\mathbf{u}$ is a known velocity field, and the unknown q is the tracer to be transported. The solution of (1) should respect two significant properties: (i) positivity must be preserved, and (ii) smearing at internal and boundary layers should not be excessive. These properties are extremely important in the context of transport in the atmosphere. Both limited-area and global atmospheric models for weather prediction need monotonic advection of tracers and moisture variables, otherwise the wrong amount of precipitation would be forecasted. Simple microphysics schemes, such as Kessler [1], require three variables (water vapor, cloud water, and rain), whereas more sophisticated parameterizations include additional variables such as ice and snow [2]. Similarly, climate models require transport of hundreds of tracers, each representing a different chemical species. Regardless of the physical scales of the model, tracers must remain positive since the physical parameterizations that govern sub-grid scale processes such as auto-conversion and sedimentation, implicitly assume such a condition. These issues have been addressed for both transient and stationary problems (See, e.g., [3]) and, in the context of finite element methods, so-called *stabilized* methods have been an active topic of research since their introduction in the early 1980s with the Streamline-Upwind method of Hughes and Brooks [4]. In this paper we address the problem of solving (1) by high-order spectral element methods without losing the ability to approach a monotone solution to the problem. Higher-order accuracy, in fact, comes at the price of aliasing phenomena in the solution ([5]), but the anti-aliasing filters typically used to give a stable spectral element solution do not respect the two conditions described above. Therefore, to achieve monotonic results with high-order spectral elements, we consider stabilization methods originally devised for finite elements, and focus on methods that can be derived directly from *subgrid scale* considerations as originally defined in [6] and [7] in the context of variational multiscale methods. These techniques assure stability by designing a diffusion-type term that is added to the Galerkin formulation of the original problem.

The first stabilized schemes based on the addition of a diffusive stabilization term to the Galerkin equation are the *Artificial Viscosity* methods

(AV) [8] and the *Streamline-Upwind* method (SU) [4]. AV, as *Hyper-viscosity* (HV), is often used in atmospheric and ocean modeling due to the property of preserving the correct energy cascade in simulations that involve turbulence. The SU scheme uses the information in the direction of the flow to add viscosity only in the streamline direction. Both methods use a constant diffusion coefficient that does not typically change from element to element. A major improvement came by introducing the residual of the governing equation in the definition of the stabilization term. When the computed solution approaches the exact solution, the stabilization term should vanish. These schemes, which are *consistent* in that the stabilization terms goes to zero as the numerical solution approaches, are considered in this paper. The most commonly used are the *Upwind-Streamline/Petrov-Galerkin* (SUPG) and the *Galerkin/Least-Squares* (GLS), devised in 1982 [9] and 1989 [10], respectively, as a consistent counterpart to SU. GLS was designed as a generalization of SUPG, but in the limit of pure advection, or for piece-wise linear elements, the GLS and SUPG methods are equivalent. Stability analysis for these two methods is detailed in [11, 12, 10]. The *Gradient Galerkin/Least-Squares* [13] for advection-diffusion with a reaction term, or the *Unusual Stabilized Finite Element Method* (USFEM) [14, 15] are a few examples. In the framework of high order methods, Petrov-Galerkin stabilization was applied by Pasquarelli and Quarteroni [16] to stabilize the convection-diffusion equation with the spectral method. Canuto used bubble functions to address the same issue [17] (See also [18, 19]).

The analyses of Hughes [6], Hughes and Stewart [20], and Hughes et al. [7] form the unifying theory of all stabilized finite element methods. Stabilized methods are subgrid scale models where the unresolved scales are intimately related to the instabilities at the level of the resolved scales, and thus should be used in the construction of the stabilization term. These schemes are known as *Variational Multiscale (VMS)* methods. Details are given in subsection 2.2.2. VMS methods are all residual-based methods that improve the stability properties of the solution, and preserve the accuracy of the underlying numerical scheme [21]. However, Godunov's theorem [22] implies that the latter property may be violated in the proximity of discontinuities or strong gradients. As already observed by Hughes, Cottrell, and Bazilevs in [21], where *NURBS* were used as high-order basis functions, unexpected convergence to monotone results were obtained independently of the order of the polynomials used. Neither SUPG, GLS, nor VMS, however, preclude the formation of over- and under-shoots in the proximity of sharp gradients of the solution. For this reason, *shock capturing* or *discontinuity dissipation* techniques, also referred to as *Spurious oscillations at layers di-*

minishing methods (SOLD) are used in combination with SUPG and VMS to introduce an additional term to the stabilized form of the equation. This issue was treated for the first time in [23], where details on how to build the stabilization parameter are also given, and in [24] for non-linear problems. A detailed review of most existing SOLD schemes can be found in a two-part paper by John and Knobloch [25, 26], where a modification of the *discontinuity-capturing* of Codina [27] is presented and is shown to be a promising option for FE solutions characterized by boundary layers.

All these methods strongly depend on a stabilization parameter that will be identified by τ throughout the paper. It will be also referred to as *intrinsic time*. A classical result was obtained by Franca, Frey and Hughes in [28] by error analysis. Their result was reproduced by other authors using different approaches. Additional expressions for τ were found by Codina in [29, 30], by Codina, Oñate and Cervera in [31], by Harari and Hughes in [13], and by Shakib, Hughes and Johan in [32], who based the derivation on the (discrete) maximum principle. Another expression is due to Franca and Valentin [15] who based their derivation on convergence and stability analysis. Starting with the formalization of VMS methods by Hughes [6], τ has often been derived using Green's functions, a thorough analysis of which is done by Hughes and Sangalli in [33]. Recently, Houzeaux, Eguzkitza and Vázquez [34] proposed a new way to derive the approximate subgrid scale solution, with results that are comparable to those of Hauke and García-Olivares in [35]. In [36], Codina builds τ using the Fourier analysis of the problem; however, the correct choice of τ remains an open problem. For this reason, we propose τ for higher-order spectral elements and use it to construct an appropriate stabilization method. To further improve the solution, we combine VMS stabilization with a p-adaptivity algorithm. p-adaptivity (see, e.g., [37, 38]) adjusts the order of the polynomial interpolation instead of modifying the computational grid. In this paper we use it in combination with VMS in those regions where discontinuities cause the high-order solution to be affected by Gibbs oscillations.

1.1. Main contribution of this paper

The main problem that we want to solve with the work presented here is that of stabilizing the spectral element solution of advection-dominated problems by sub-grid scale stabilization techniques (namely, VMS), and improve the solution by reducing the under- and overshoots that would occur if classical filters were to be used. The definition and implementation of τ in VMS stabilization may greatly affect the result. We hence adapted the

method described in [34] to compute τ, and applied it to spectral elements that use Legendre-Gauss-Lobatto (LGL) nodes, and show that this technique can be used in problems where spectral element filters fail. We finally apply polynomial adaptivity (i.e., we lower the order of interpolation by keeping the computational grid untouched), only where the solution is characterized by a propagating discontinuity. The combination of VMS, shock capturing and p-adaptive methods will be shown to be an encouraging direction to take for constructing high-order positive-definite spectral element methods. To assess the algorithm, steady and transient advection-diffusion problems are solved on one- and two-dimensional domains using spectral elements up to order *16*. We compare the performance of the method using the VMS against those obtained with previous classical SE schemes.

1.2. Outline of this paper

The remainder of the paper is organized as follows. After this introduction, the numerical method and the corresponding stabilization are derived in Sections 2 and 3. Tests to verify the algorithm and a discussion of the results are presented in Sections 4 and 5, respectively.

2. Numerical method

Given the space L^2 of real-valued functions that are square integrable in a bounded domain $\Omega \subset \mathbb{R}^2$ with boundary Γ, the Sobolev space H^1 of weakly-differentiable functions will be used. Specifically, $W \subseteq H^1$ represents the space of trial and basis functions of the Galerkin formulation to follow. In L^2 the inner product is given by $(\cdot,\cdot)$, and the *2*-norm associated with the space is denoted by $\|\cdot\|_2$. For simplicity, we add the property that the solution q vanishes on the boundary $\partial\Omega$; under this assumption, $W \subseteq H^1_0$. Given a finite element partition $\Omega_h = \bigcup_{i=1}^{n_{el}} K_i$ of the computational domain Ω into n_{el} high-order conforming quadrilaterals of characteristic length h, W^h is the finite dimensional set derived from W. The discrete weak form reduces to the problem of finding the function $q^h \in (W^h; 0, t)$ such that

$$(\psi^h, \frac{\partial q^h}{\partial t}) + a(\psi^h, q^h) = (\psi^h, f) \qquad \forall\, \psi^h \in W^h \tag{2}$$

where, after integrating by parts and assuming homogeneous Dirichlet boundary conditions, we define:

$$(\psi^h, \frac{\partial q^h}{\partial t}) \doteq \int_{\Omega_h} \psi^h \frac{\partial q^h}{\partial t}\, d\Omega_h,$$

$$a(\psi^h, q^h) \doteq \int_{\Omega_h} \psi^h \mathbf{u} \cdot \nabla q^h \, d\Omega_h + \int_{\Omega_h} \nu \nabla \psi^h \cdot \nabla q^h \, d\Omega_h,$$

$$(\psi^h, f) \doteq \int_{\Omega_h} \psi^h \, f \, d\Omega_h = 0.$$

Integrals are constructed within a Galerkin framework via

$$\int_{\Omega_h} (\cdot) \, d\Omega_h = \sum_{el=1}^{n_{el}} \int_{\Omega_{el}} (\cdot) \, d\Omega_h^{el} \, .$$

Remark 1: If advection dominates diffusion, unless $h < \nu$ or the exact solution is globally smooth, the Galerkin approximation expressed by (2) is such that q^h will suffer from severe/unacceptable oscillations [11, 39]. Furthermore, if the discretization relies on high-order methods, Gibbs oscillations may occur regardless of the size of the grid. Different ways to improve stability will be described in the following sections.

2.1. The spectral element method

The weak form in Eq. (2) is used with quadrilateral elements of order p, where the element-wise solution q^h is approximated by the expansion $\sum_{k=1}^{N_p} \Psi_k(\mathbf{x}) \, q_k^h(t)$ on $N_p = (p+1)^2$ collocation points within the element. The expansion functions Ψ_k are constructed as the tensor product from the Lagrange polynomials $h_i(\xi(\mathbf{x}))$ and $h_j(\eta(\mathbf{x}))$ of order p as:

$$\Psi_k(\mathbf{x}) = h_i(\xi(\mathbf{x})) \otimes h_j(\eta(\mathbf{x})), \quad \forall \, i, j = 1, ..., p+1. \tag{4}$$

$h_i(\xi(\mathbf{x}))$ and $h_j(\eta(\mathbf{x}))$ are the polynomials associated with the LGL points ξ_i and η_j, respectively. The LGL points are the zeros of

$$(1 - \xi^2) P_N^{'}(\xi) = 0$$

where P_N' is the derivative of the N^{th}-order Legendre polynomial. Quadrature is performed on the reference element $\hat{\Omega}^h = [-1, 1]^2$ with LGL points that have quadrature weights ω. Substitution of the expansion $\sum_{k=1}^{N_p} \Psi_k(\mathbf{x}) \, q_k^h(t)$ into the weak form (2) yields the semi-discrete (in space) matrix problem

$$\mathbf{M} \frac{\partial \mathbf{q}^h}{\partial t} + \mathbf{A}\mathbf{q}^h + \mathbf{D}\mathbf{q}^h = 0 \tag{5}$$

where $\mathbf{q}^h$ is the array of the unknowns on the grid points, and $\mathbf{M}$, $\mathbf{A}$, and $\mathbf{D}$ are the global mass, advection, and diffusion matrices, respectively. These matrices are obtained from the direct stiffness summation (DSS) of the elemental matrices $\mathbf{M}^{el}$, $\mathbf{A}^{el}$, and $\mathbf{D}^{el}$ given by:

$$\mathbf{M}^{el}_{kl} = \int_{\Omega^{el}} \Psi_k \Psi_l \, d\Omega_{el} \tag{6a}$$

$$\mathbf{A}^{el}_{kl} = \int_{\Omega^{el}} \mathbf{u} \cdot \nabla \Psi_k \, \Psi_l \, d\Omega_{el} \tag{6b}$$

$$\mathbf{D}^{el}_{kl} = \int_{\Omega^{el}} \nu \nabla \Psi_k \cdot \nabla \Psi_l \, d\Omega_{el}. \tag{6c}$$

The mass matrix $\mathbf{M}$ is diagonal assuming inexact integration.

All the integrals defined above are approximated by the quadrature formula

$$\int_{\Omega^h_{el}} (\cdot) d\mathbf{x} = \int_{-1}^{1} \int_{-1}^{1} \hat{(\cdot)} |J(\xi,\eta)| d\xi \, d\eta \approx \sum_{i=1}^{p+1} \sum_{j=1}^{p+1} \hat{(\cdot)} |J(\xi,\eta)| \omega_i \omega_j, \tag{7}$$

where J is the Jacobian matrix associated with the map between the physical element $\Omega^h(x,y)$ and the reference element $\hat{\Omega}^h(\xi,\eta)$. The integration is exact up to polynomials of order *2p-1*. The *p+1 LGL* points lie along the edges and in the interior of the elements. For more on SEM see, e.g., [40, 38].

We solve the linear system of ordinary differential equations (5) with an appropriate strong-stability preserving (SSP) time integrator. In particular, we use a five-stage explicit *third-order Runge-Kutta* method (RK35) [41]. SSP methods avoid the production of additional oscillations or damping.

From 3^{rd}-order and up, the disposition of the nodes of spectral elements differ from classical finite elements in the way represented in Figure 1 for a 4^{th}-order element.

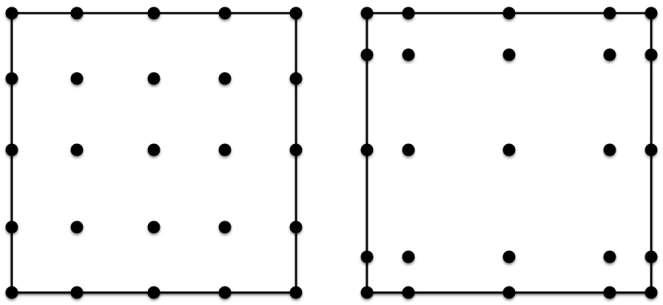

Figure 1: Nodes disposition for 4^{th}-order FE (left), and SE (right).

2.2. Stabilization techniques

Aliasing and Gibbs oscillations render the Galerkin solution of (1) unstable since unwanted oscillations will pollute the numerical solution. In the framework of spectral elements, the common strategy to control these oscillations is the use of anti-aliasing filters (See, e.g., [42, 43, 44, 38, 45] and references therein). Filtering, however, suffers from non-positivity that is unacceptable in most problems that involve transport. A suitable alternative to filters may be the use of a stabilized spectral element approximation based on a residual-based diffusion-like term added to the left hand-side (*LHS*) of (2). A stabilization technique should have the important property of consistency (for instance, artificial diffusion stabilizes but is not necessarily consistent). Thus, the additional viscous term should vanish as the size of the element approaches zero. The stabilized counterpart of (2) is:

$$(\psi^h, \frac{\partial q^h}{\partial t}) + a(\psi^h, q^h) + b(\psi^h, q^h) = (\psi^h, f) \qquad \forall\, \psi^h \in W_h, \tag{8}$$

where $b(\psi^h, q^h)$ is the stabilization term.

A general method for finding τ does not exist, and different choices for τ dramatically influence the accuracy of the solution. The literature on the optimal selection of τ is vast, and we refer to [25, 26] for a comprehensive analysis of different definitions.

Table 1: Stabilized methods

Method	$b(\psi^h, q^h)$	$\mathcal{L}(\psi^h)$
AV/HV	$\int_{\Omega_h} \mathcal{L}(\psi^h)\bar{\nu}\left[\nabla^\alpha q^h\right]\, d\Omega_h$	$\mathcal{L} = \nabla^\alpha \psi^h$
SU	$\int_{\Omega_h} \mathcal{L}(\psi^h)\bar{\nu}\left[\mathbf{u}\cdot\nabla q^h\right]\, d\Omega_h$	$\mathcal{L} = \mathbf{u}\cdot\nabla\psi^h$
SUPG	$\int_{\Omega_h} \mathcal{L}(\psi^h)\tau\left[\frac{\partial q^h}{\partial t} + \mathbf{u}\cdot\nabla q^h - \nu\Delta q^h - f\right]\, d\Omega_h$	$\mathcal{L} = \mathbf{u}\cdot\nabla\psi^h$
GLS	$\int_{\Omega_h} \mathcal{L}(\psi^h)\tau\left[\frac{\partial q^h}{\partial t} + \mathbf{u}\cdot\nabla q^h - \nu\Delta q^h - f\right]\, d\Omega_h$	$\mathcal{L} = \mathbf{u}\cdot\nabla\psi^h - \nu\Delta\psi^h$
VMS	$-\int_{\Omega_h} \mathcal{L}^*(\psi^h)\tau\left[\frac{\partial q^h}{\partial t} + \mathbf{u}\cdot\nabla q^h - \nu\Delta q^h - f\right]\, d\Omega_h$	$\mathcal{L}^* = -\mathbf{u}\cdot\nabla\psi^h - \nu\Delta\psi$

In table 1, $\bar{\nu}$ indicates a constant diffusion coefficient, and $\alpha = \beta/2$, where β is a positive even power of the hyper-viscosity operator ($\beta = 2$ yields the usual AV). Although HV is scale-selective (i.e., it damps only higher frequencies), it is not consistent, nor is it physical. In fact, to maintain the correct physical dimensions of the hyper-viscous operator, the value of the diffusivity coefficient $\bar{\nu}$ must be different when different α are used. Its selection is hence not trivial. Furthermore, as Figure 20-*d* indicates, the diffusion is isotropic and spatially homogeneous. The operator does not incorporate the problem's physics.

The method of Douglas and Wang (DW) [46] was omitted as it can be included into the VMS method, although its derivation was specifically done in the context of Stokes problems rather than scalar advection-diffusion. The SUPG and VMS will be described in the following subsections.

2.2.1. Streamline-upwind/Petrov-Galerkin (SUPG)

The SUPG method was designed by Brooks and Hughes [9] and was later generalized for multidimensional problems by Hughes and Mallet [47]. It is a consistent alternative to the artificial diffusion approach or to the overly diffusive streamline upwind (SU) method. Its use has been ubiquitous in the solution of transport problems by the finite element method (See, e.g., [48, 28, 49, 50, 51]). The application of this strategy to higher-order schemes was first tested for spectral methods by Canuto and coworkers in [17, 18, 19, 52], and later by Hughes and coworkers in [21] using *non-uniform rational B-splines* (NURBS). In this paper we show its properties when used with high-order spectral elements. SUPG is a Petrov-Galerkin method in

that it does not assume that the basis and test functions live in the same space. We introduce the additional space Ψ^h of test functions w^h defined by

$$\Psi^h \doteq \left\{ w^h \,:\, w^h = \psi^h + \tau \mathbf{u} \cdot \nabla \psi^h \,:\quad \psi^h \in W^h \right\}.$$

We have the problem of finding the function $q^h \in (W^h; 0, t)$ such that

$$(\psi^h + \tau \mathbf{u} \cdot \nabla \psi^h, \frac{\partial q^h}{\partial t}) + a(\psi^h + \tau \mathbf{u} \cdot \nabla \psi^h, q^h) = (\psi^h + \tau \mathbf{u} \cdot \nabla \psi^h, f) \qquad \forall\, \psi^h \in W_h. \tag{9}$$

Rearrangement of (9) yields

$$\underbrace{(\psi^h, \frac{\partial q^h}{\partial t}) + a(\psi^h, q^h) - (\psi^h, f)}_{\text{Galerkin}} + b(\psi^h, q^h) = 0 \qquad \forall\, \psi^h \in W_h \tag{10}$$

where

$$b(\psi^h, q^h) \doteq \int_\Omega \left[\frac{\partial q^h}{\partial t} + \mathbf{u} \cdot \nabla q^h - \nu \Delta q^h - f \right] \tau\, \mathbf{u} \cdot \nabla \psi^h \, d\Omega_h \tag{11}$$

is the stabilizing term. In (11), $\partial_t q^h + \mathbf{u} \cdot \nabla q^h - \nu \Delta q^h - f$ is the residual of the governing equation, and $\tau \in L^\infty$ is the stabilization parameter.

2.2.2. The variational subgrid scale formulation (VMS)

Following [33], we define the idempotent linear projector $\mathcal{P}$ such that $Range(\mathcal{P}) = \bar{W} \subset W$, and such that $\bar{\psi} \in \bar{W}$ is the projection of $\psi \in W$ given by $\bar{\psi} = \mathcal{P}\psi$. If we denote $\bar{W}$ as the space of resolved scales, and build the space W' that completes $\bar{W}$ in W and that we will call the space of subgrid scales, we have $W = \bar{W} \oplus W'$, where $\oplus$ is the overlapping sum decomposition of the two spaces. Using the properties of $\mathcal{P}$, the definition of W, and the linear independence of $\bar{W}$ and W', we decompose the weak form (2) into

$$\left(\bar{\psi}, \frac{\partial \bar{q}}{\partial t}\right) + \left(\bar{\psi}, \frac{\partial q'}{\partial t}\right) + a(\bar{\psi}, \bar{q}) + a(\bar{\psi}, q') = (\bar{\psi}, f) \tag{12a}$$

$$\left(\psi', \frac{\partial \bar{q}}{\partial t}\right) + \left(\psi', \frac{\partial q'}{\partial t}\right) + a(\psi', \bar{q}) + a(\psi', q') = (\psi', f). \tag{12b}$$

We back-integrate by parts the bilinear forms $a(\cdot,\cdot)$ in (12) that depend on the subgrid scales, yielding

$$\left(\bar{\psi}, \frac{\partial \bar{q}}{\partial t}\right) + \left(\bar{\psi}, \frac{\partial q'}{\partial t}\right) + a(\bar{\psi}, \bar{q}) - \int_{\Omega_h} q' \mathcal{L}^*(\bar{\psi})\, d\Omega_h = (\bar{\psi}, f) \tag{13a}$$

$$\left(\psi', \frac{\partial \bar{q}}{\partial t}\right) + \int_{\Omega_h} \psi' \mathcal{L}(q')\, d\Omega_h + \int_{\Omega_h} \psi' \mathcal{L}(\bar{q})\, d\Omega_h = (\psi', f), \tag{13b}$$

where all the boundary fluxes and subscales vanish on the boundary, and $\mathcal{L}^* := -\frac{\partial}{\partial t} - \mathbf{u}\cdot\nabla - \nu\Delta q$ is the adjoint operator of $\mathcal{L}$. Equating the integrands in (13b), we obtain:

$$\mathcal{L}(q') = f - \mathcal{L}(\bar{q}), \tag{14}$$

where the time-dependent contributions are included in $\mathcal{L}$. The solution of (14) for q' must be inserted into (13a) to compute the large-scale solution $\bar{q}$ by means of the finite or spectral element method.

One fundamental step in the derivation of the subgrid scales is the approximation of q' from Equation (14). In the context of high-order spectral elements with non-equispaced nodes, we adopt the approach of Houzeaux, Eguzkitza, and Vázquez [34]), who used bubble functions to approximate q' in the solution of equation (13b). To do this, we use (14) and re-express (13b) using the space of bubbles that vanish at the nodes of every element. We have:

$$\int_{\Omega_h} \psi' \mathcal{L}(q')\, d\Omega_h = \int_{\Omega_h} \psi'\, R(\bar{q})\, d\Omega_h \quad \forall \psi' \in W_0', \tag{15}$$

where $R(\bar{q}) = \partial_t q^h + \mathbf{u}\cdot\nabla q^h - \nu\Delta q^h - f$ is the residual of the governing equation, and W_0' indicates the space of bubbles (i.e., subgrid-scale functions that are zero at the element nodes, and hence ensure nodal exactness of the numerical solution). We omitted the time-dependent terms since we used a sufficiently small Δt. (15) implies the strong form

$$\mathcal{L}(q') = R(\bar{q}), \tag{16}$$

to be solved for q' with Dirichlet boundary conditions: $q'(0) = 0$ and

$q'(h) = 0$, on every element of length h. Using the residual-free bubble $b(x)$ ([53, 54]), we substitute the expression $q'(x) = b(x)R(q^h)$ into (15) and solve for $b(x)$ with boundary conditions $b(0) = 0$ and $b(h) = 0$. We have: $\mathcal{L}(b(x)R(q^h))\, d\Omega_h = R(\bar{q^h})$. To proceed, we assume that $R(q^h)$ is constant (i.e., we can think that $R(q^h)$ is always known from the previous time-step), and take it out of the operator $\mathcal{L}(\cdot)$. This yields $\mathcal{L}(b(x)) = 1$, that, for the one-dimensional steady-state advection-diffusion equation

$$u\, b_x(x) - \nu\, b_{xx}(x) = 1, \tag{17}$$

has solution

$$b(x) = \frac{x}{u} + \frac{h}{u}\frac{1 - e^{xu/\nu}}{e^{hu/\nu}}. \tag{18}$$

For linear elements, h is simply the length of the element. For higher-order finite elements, h becomes a fraction of the total element size h if the internal nodes are equispaced. In the case of spectral elements, where the LGL points are unevenly distributed, (18) is computed by using h as the local distance between two consecutive points. The distributin of $b(x)$ along the element is represented in Figure 2. We use the approximation $q' \approx \tau \mathbf{R}$ with τ defined in (23), substitute it into (13a) to find the VMS (or generalized) stabilized method

$$\boxed{\left(\bar{\psi}, \frac{\partial \bar{q}}{\partial t}\right) + a(\bar{\psi}, q) - \int_{\Omega_h} \mathcal{L}^*(\bar{\psi})\, \tau\, \mathbf{R}(\bar{\mathbf{q}}) d\Omega_{el} = (f, \bar{\psi}).} \tag{19}$$

Eq. (19) differs from the weak form in Eq. (2) by the addition of a stabilization term which models subgrid scales. The additional third term is the viscous-like contribution that stabilizes the equation.

Observations on time-dependent subgrid-scales: The time-dependent approximation (13) includes a contribution from the time evolution of the subscales given by $\partial_t q'$. This may require tracking of the subscales in the time integration, unless the hypothesis of *quasi-static subscales* (i.e. $\partial_t q' \approx 0$) is applied (See [36] for details). Under this hypothesis, the contribution from the subgrid scales only appears in the steady part of the Galerkin approximation. If a sufficiently small time-step is used with an

explicit time integrator, we do not lose accuracy with the quasi-static hypothesis. With the use of large time-steps with semi-implicit time integrators in atmospheric simulations, tracking of the subscales is hence needed. This issue is reserved for future work by the authors.

Remark 3: It must be pointed out that, for the solution of the scalar transport equation, the expressions for SUPG and VMS are the same. Any difference is caused by a different definition of τ.

2.3. The intrinsic time τ

A standard intrinsic time τ for finite elements was derived by Franca, Frey and Hughes [28]:

$$\tau = \frac{h_k}{2||\mathbf{u}||_2}\xi(Pe_k) \tag{20}$$

where ξ is a function of the *Peclet* number Pe_k which relates the advection effects with respect to diffusion via:

$$Pe_k = m_k \frac{h_k||\mathbf{u}||_2}{2\nu}. \tag{21}$$

In (21) m_k is an algorithmic constant that should contain information regarding the interpolating functions. For linear elements, one definition of ξ was derived using nodal exactness in [9], i.e. the finite element solution using ξ defined in this way is equivalent to the analytic solution at the nodes of the finite element mesh of a one dimension problem. In the context of subgrid scale approximations, this condition is satisfied when the subgrid scales are zero on the element nodes. We write:

$$\xi(Pe_k) = \coth(Pe_k) - \frac{1}{Pe_k}. \tag{22}$$

A whole set of definitions of ξ appears in the literature: see a review in [34]); for systems of PDEs, see [55].

2.3.1. τ for spectral elements

It is assessed that for one-dimensional linear elements, a subgrid scale method gives nodally exact results if h_k is the full distance between the boundary nodes of the element. To derive it in the context of higher-order spectral elements with non-equispaced nodes, we extend the approach of Houzeaux, Eguzkitza, and Vázquez [34] developed for quadratic and cubic

one-dimensional finite elements, using bubble functions in the approximation of the subgrid scales to solve equation (13b). The stabilization parameter τ is built inside the element as a function of the bubbles on every segment delimited by two consecutive nodes. We write:

$$\tau_i^{i+1} = \frac{1}{x_{lgl}(i+1) - x_{lgl}(i)} \int_{x_{lgl}(i)}^{x_{lgl}(i+1)} b(x)\, dx, \tag{23}$$

where $x_{lgl}(i+1)$ and $x_{lgl}(i)$ are the coordinates of two consecutive LGL points. Using (23), the stabilization integral is decomposed into a summation of all the contribution of the subelements $[x_{lgl}(i+1) - x_{lgl}(i)]$. Uniform spacing implies uniform τ for each sub-element. The uneven spacing of the element nodes is the major difference with respect to the definitions derived in previous studies. In this case the intrinsic time is non-uniform along the element, as it appears in Figure 2, where bubbles and the corresponding τ are displayed for an element of order 7. We expand τ using the Galerkin approximation

$$\tau = \sum_{k=1}^{p+1} \tau_k \psi_k, \tag{24}$$

where $\psi_k \in \Psi^h$ are the same basis function previously introduced in the approximation of the solution by spectral elements. The coefficients τ_k correspond to the value of τ at node k and whose value is obtained by (23). This step allows the algorithm to maintain the simplicity similar to linear elements in that we are using one stabilization integral along the element; however, the characteristics of the non-uniform grid are incorporated into the method. Throughout the paper we use τ in (23) for all our simulations.

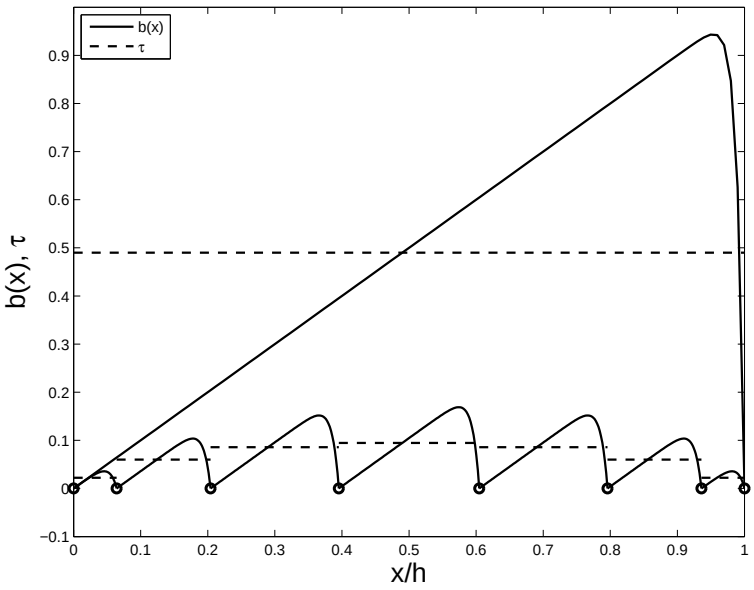

Figure 2: Bubbles $b(x)$ and τ for a 7^{th}-order unitary spectral element. The biggest bubble in the plot is the bubble that a linear element would have.

2.4. Spurious oscillations at layers diminishing (SOLD) methods

Methods in the form of (19) may produce overshoots and undershoots in the proximity of an internal or boundary layer. These unwanted oscillations can be suppressed, without affecting the global solution, by adding an additional diffusive term of the form

$$(\nabla\psi^h, \tilde{\tau}\nabla q^h), \tag{25}$$

where consistency must be respected through a proper construction of $\tilde{\tau}$. We would like to have a method that does not modify the diffusion in the streamline direction since that is already accounted for by the stabilization term, but also avoids overdamping in the crosswind direction. The comprehensive set of tests performed by John and Knobloch reveals that Codina's [27] is among the best methods that satisfy these conditions when used with finite elements. In [27], $\tilde{\tau}$ is defined by:

$$\tilde{\tau} = \frac{1}{2}\max\left\{0, C - \frac{2\nu}{|\mathbf{u}_{||}|h_k}\right\} h_k \frac{|R(q^h)|}{||\nabla q^h||}\left(\mathbf{I} - \frac{\mathbf{u}\otimes\mathbf{u}}{|\mathbf{u}|^2}\right) \tag{26}$$

where C is a constant, $\mathbf{u}_{||}$ is the velocity component in the streamline direction, and $\otimes$ indicates a tensor product. Codina suggests $C = 0.7$ for linear and bilinear elements, and $C = 0.35$ for quadratic and biquadratic elements. However, for higher order elements using LGL points, we found that the best results were obtained by setting $C = 1$, as long as h_k is selected properly in the construction of both $\tilde{\tau}$ and τ_k.

An alternative to (25) comes from Johnson, Schatz, and Wahlbin [56] who defined the following:

$$\left(\tilde{\tau}\mathbf{u}^{\perp}\cdot\nabla\psi^h, \mathbf{u}^{\perp}\cdot\nabla q^h\right), \qquad \mathbf{u}^{\perp} = \frac{(-w,u)}{|\mathbf{u}|}. \tag{27}$$

In the current work, (27) gives better results than (25), and was then used throughout. The results obtained with this technique are labeled with *DC* for *Discontinuity Capturing*.

3. *p*-adaptivity

p-adaptivity is one additional tool that can further help the suppression of Gibbs oscillations. The concept is simple and is easily coded on structured grids. It consists of identifying the position of discontinuous solutions, and dropping the order of discretization to 1^{st} for all the elements that fall within the discontinuity. The discontinuity is sought with a proper error estimator. The simple physics of the advection-diffusion problems discussed below allows for the energy-norm of the gradient of the solution to be a sufficiently good estimator for the current study. However, more advanced methods should be considered. Algorithm 1 is a simple implementation of this concept within our code. The overhead is none because the number of loop operations does not change with respect to the original case where high-order elements are used everywhere. Clearly, the algorithm can be easily optimized, but we present the pseudo-code below for the sake of clarity. The method was applied to a two-dimensional advection-diffusion problem with internal and boundary layers in a skew velocity field. Results are shown in Figure 9.

4. Numerical testing

The algorithms discussed in Section 2 were tested using standard problems described in the literature of stabilized finite element methods for the

Algorithm 1 Compute the 1^{st}-order rhs

```
// Loop over all elements (iel) of the high-order computational grid :
for iel = 1 to nelem do

  // Check if the element contains a discontinuity:
  if iel is s.t. ||∇q_h||_2 > ε then

    // Treat element iel as a grid of (ngl − 1) × (ngl − 1) sub-elements:
    for isubel = 1 to maximum number of sub-elements do
      Create rhs using 1st-order basis functions and integration rule
    end for

  else
    // Do as usual:
    Create rhs for the high-order spectral element.
  end if

end for
```

advection-diffusion (AD) equation:

- 1D Steady-state homogeneous advection-diffusion (*St-1D*)
- 1D Steady-state advection-diffusion with source (*St-1D-S*)
- 2D Steady-state advection-diffusion with internal and boundary layers (*St-2D*).
- 2D Time-dependent advection-diffusion with "L"-shaped discontinuity (*Tr1-2D*).
- 2D Time-dependent advection of a sharp tracer in a doubly periodic channel (*Tr2-2D*).

St-1D:. One-dimensional steady-state advection-diffusion. The tracer q_h is propagated with constant velocity $u = 1\,m\,s^{-1}$ and diffusivity $\nu = 1/512\,m^2\,s^{-1}$ first on two elements of order $p = 10$ (Figure 3), and then on four elements of order $p = 12$ (Figure 4). The domain is the line segment $\Omega = [-1, 1]$ with Dirichlet boundary conditions $q_h(-1) = 0$ and $q_h(1) = 1$. We compared the filtered (top row) against the stabilized solution (bottom row) and observe a decrease of oscillations and undershoots. Also, at higher order and

finer resolution, the capabilities of the filter are clearly being challenged by the presence of the boundary layer at $x = 1$. At the same time, small oscillations near the nodes of the element by the boundary layer are not completely suppressed by the stabilized method either; hence, additional localized smoothing is sought.

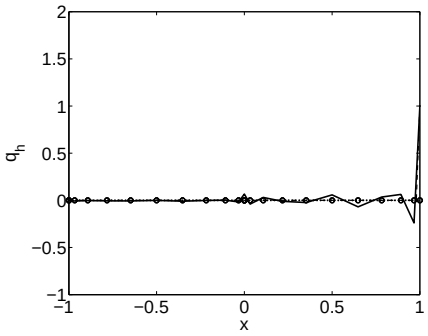

(a) Filter. 2 el, p = 10

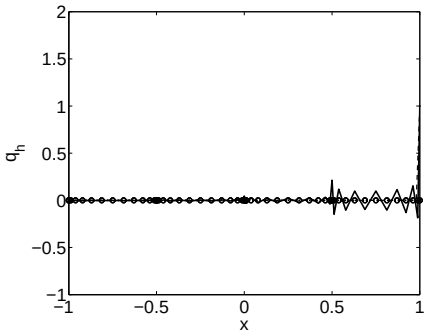

(a) Filter. 4 el, p = 12

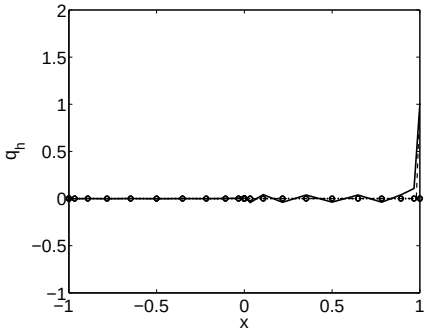

(b) VMS. 2 el, p = 10

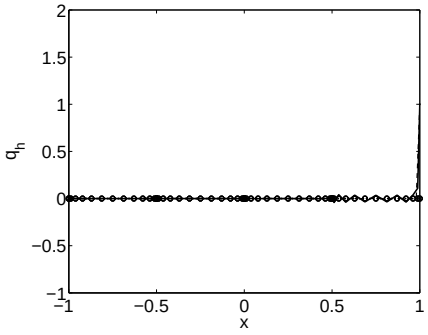

(b) VMS. 4 el, p = 12

Figure 3: *St-1D*: $\nu = 1/512\, m^2\, s^{-1}$. The exact solution is dashed. The circles indicate the grid points.

Figure 4: *St-1D*: $\nu = 1/512\, m^2\, s^{-1}$. The exact solution is dashed. The circles indicate the grid points.

St-1D-S:. Steady state advection-diffusion with source term $f = 1$. q_h is propagated with constant velocity $u = 1\, m\, s^{-1}$ and two different diffusivities: $\nu = 5{\times}10^{-3}\, m^2\, s^{-1}$ and $\nu = 5{\times}10^{-2}\, m^2\, s^{-1}$. The domain is the line segment $\Omega = [0, 1]$ and homogeneous Dirichlet boundary conditions are imposed. The domain is subdivided into two elements of order $p = 16$ and runs are compared using filtered SE (top row in Figures 5 and 6), and VMS (bottom row). We observe a very similar behavior of the solution among the two different cases in the smooth problem (Figure 5). The results are comparable

to the ones obtained by Houzeaux et al. with their τ for quadratic and cubic elements in [34].

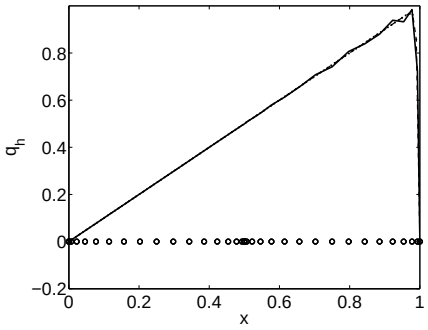

(a) Filter

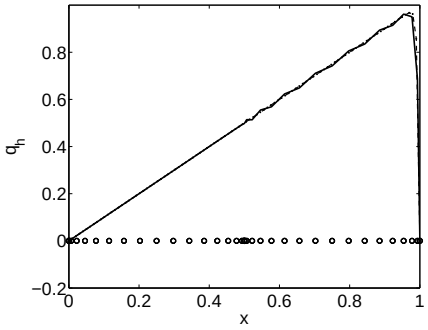

(b) VMS

Figure 5: *St-1D-S*: $\nu = 5 \times 10^{-3}\, m^2\, s^{-1}$. 2 16^{th}-order elements. The exact solution is dashed. The circles indicate the grid points.

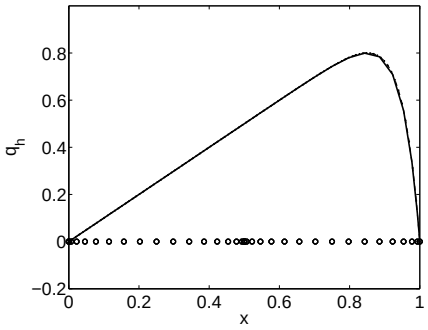

(a) Filter

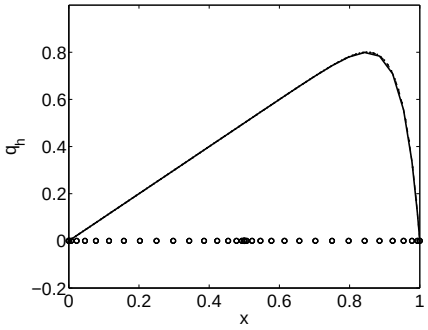

(b) VMS

Figure 6: *St-1D-S*: $\nu = 5 \times 10^{-2}\, m^2\, s^{-1}$. 2 16^{th}-order elements. The exact solution is dashed. The circles indicate the grid points.

St-2D:. Standard steady advection-diffusion skew to the mesh (e.g., [27]): a discontinuity is propagated with constant velocity $\mathbf{u} = (1, -2) m\, s^{-1}$ and diffusivity $\nu = 10^{-8}\, m^2\, s^{-1}$ in the unit square $\Omega = [0, 1] \times [0, 1]$. The initial configuration is shown in Figure 7.

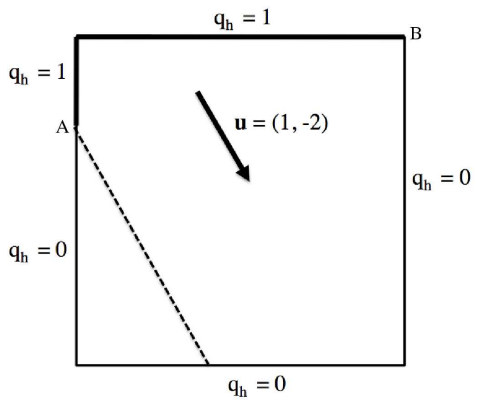

Figure 7: *St-2D*: initial configuration of the steady-state problem

Dirichlet boundary conditions are prescribed:

$$q_h = \begin{cases} 1 & \text{if} \quad y = 1, \\ 1 & \text{if} \quad x = 0 \text{ and } y \geq 0.7, \\ 0 & \text{otherwise.} \end{cases}$$

In Figures 8-12 we illustrate the run of the same case with different number of elements and order of the interpolating polynomials. For direct comparison of our solution with the ones in the existing literature of finite elements, we first run the test with linear elements ($p = 1$), and present the results in Figure 8. The multiscale solution of this problem (see Figure 8*a*) shows important boundary and internal layers that are damped with the discontinuity capturing techniques of Section 2.4. The application of the discontinuity capturing (DC) scheme greatly improves the solution and yields monotonicity (see Figure 8*b*). In Figure 9 we maintained the same number of nodes of the previous run, but increased to 4^{th} the order of interpolation to assess the algorithm in the context of this paper (i.e. 50 elements of order 4 were used instead of 200 elements of order 1). The similar behavior of the solution with respect to the 1^{st}-order polynomial run suggests that the residual-based methods as implemented in this study may not be sensitive to the distribution of the interpolation nodes within the elements edges. As it appears in Figures 9*c*, the behavior is completely analogous to the previous run. However, monotonicity is lost in two singular nodes: with reference to Figure 9*c*, the 4^{th}-order solution is smooth and monotone everywhere except for the nodes represented as points A and B in Figure 7. This is not surprising: at A and B the tracer is leaving the boundary with a skew

angle; an incorrect imposition of boundary conditions at these nodes may be causing the problem. The numerical singularity at this points should be addressed but it will not be done in the current work. These are fully suppressed by applying the p-adaptivity algorithm described above, as it is shown in Figure 9*d*.

Decreasing the number of computational nodes by doubling the order from 4 to 8 and setting the number of elements to 10 in x and z, even with a discontinuity capturing term, the solution starts to lose monotonicity. This appears in Figures 11 and 12, where extrema get larger than in the previous cases. This problem shows that the construction of the stabilizing parameter τ should include information on the order of the interpolating polynomial.

For a better view of the problem, in Figures 10 and 12 we present a vertical slice of the solution. The boundary layers are evident. Their damping, however, is clear if $VMS + DC$, and possibly p-adaptivity, are applied.

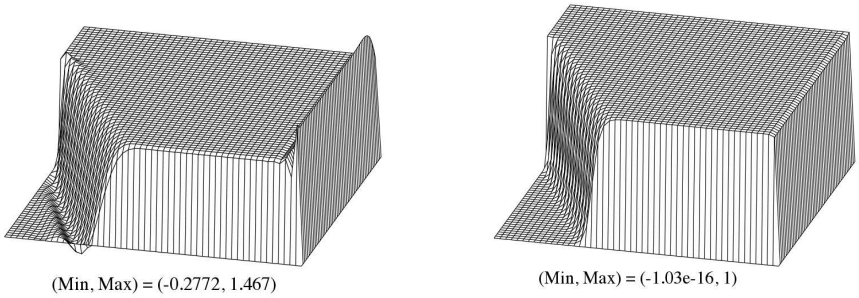

(a) VMS (b) VMS + DC

Figure 8: *St-2D*: steady-state solution on 200×200 1^{st}-order elements. (For plotting only, the data are interpolated to a 50×50 node grid using Octave [57]).

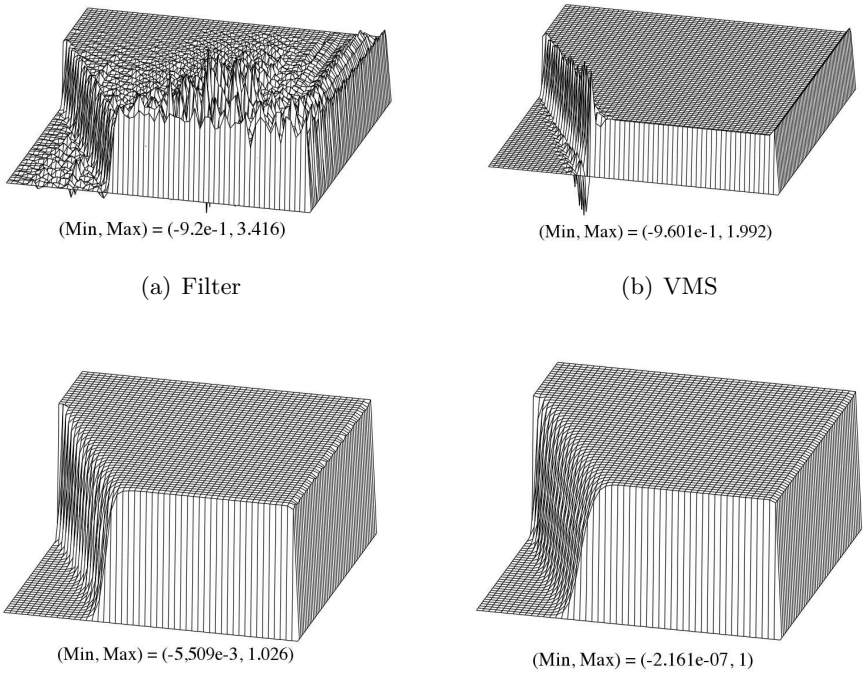

(a) Filter (b) VMS

(c) VMS + DC (d) VMS + DC + p-adaptivity

Figure 9: *St-2D*: steady-state solution on 50×50 4^{th}-order elements.

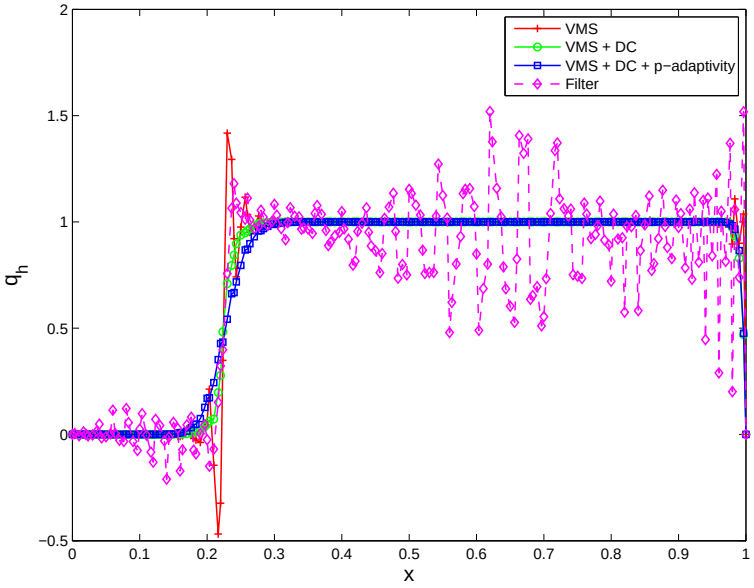

Figure 10: *St-2D*: steady-state solution on 50×50 4^{th}-order elements. Vertical slice at $z = 0.3$

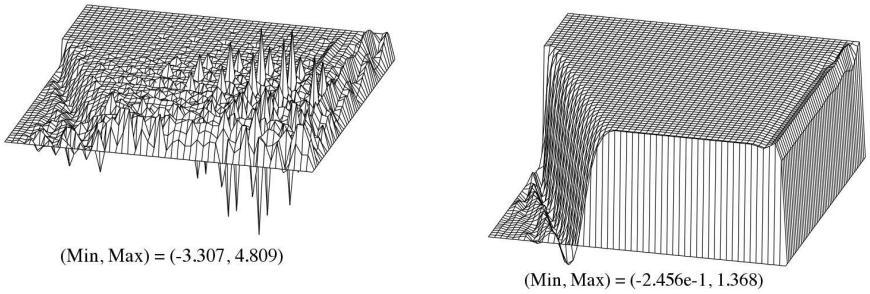

(a) Filter (b) VMS

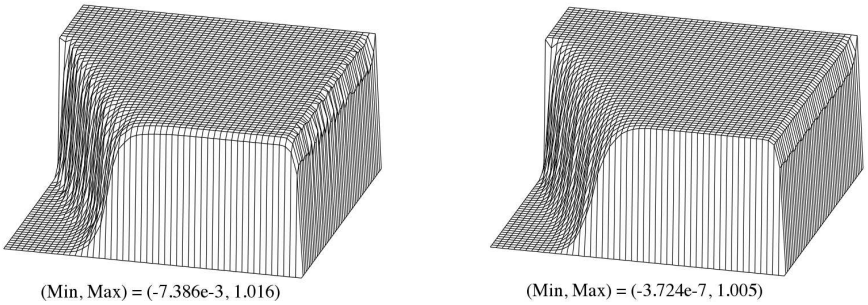

(c) VMS + DC (d) VMS + DC + p-adaptivity

Figure 11: *St-2D*: steady-state solution on 10×10 8^{th}-order elements.

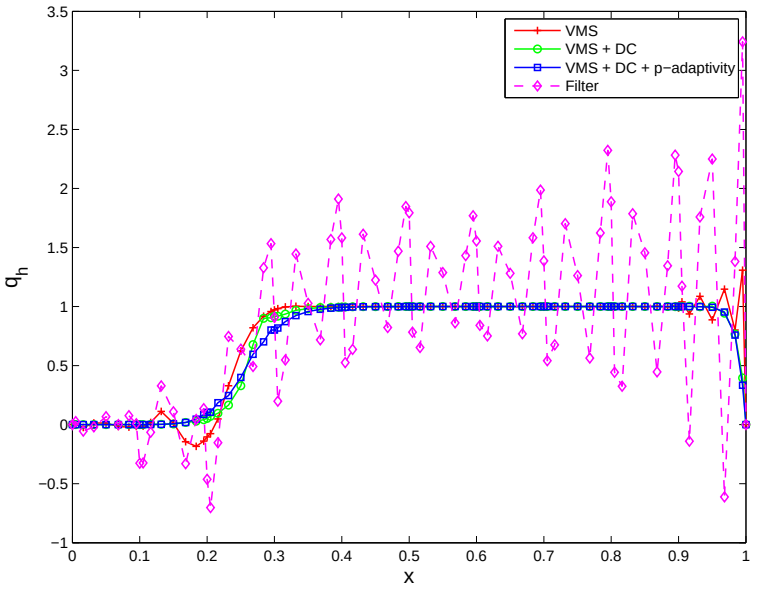

Figure 12: *St-2D*: steady-state solution on 10×10 8^{th}-order elements. Vertical slice at $z = 0.3$

Tr1-2D:. Transient advection-diffusion of an L-shaped discontinuity in a flow where $\nu = 10^{-6}\, m^2\, s^{-1}$ and the velocity $\mathbf{u}$ of magnitude $|\mathbf{u}| = 0.5\sqrt{2}\, m\, s^{-1}$ is at 45^o with respect to the axis (x, z). The initial configuration is shown in Figure 13.

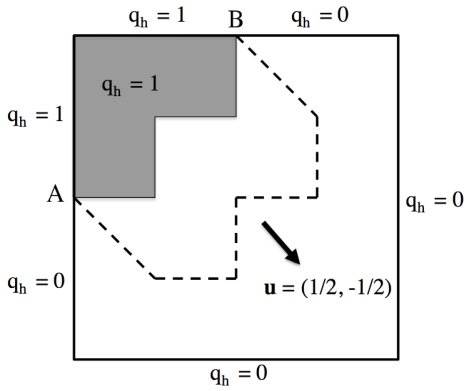

Figure 13: *Tr1-2D*: initial configuration of the L-shaped problem

The convex shape of the sharp discontinuity makes this problem more challenging than the previous case [58], and is chosen to analyze robustness

and accuracy of the algorithm. Runs were performed at two different resolutions and two different orders of interpolating polynomials. In particular we have: approx. 100 points per side using 25×25 $4^{th}-order$ elements (Figure 14), and 12×12 8^{th}-order elements (Figure 15); and approx. 200 points per side using 50×50 4^{th}-order (Figure 17), and 25×25 8^{th}-order (Figure 17). In the figures, *Filter* means that the SEM solution was filtered at every time-step. *VMS* and/or *DC* indicate that the SEM solution is stabilized by the VMS with or without a discontinuity capturing term (DC). *VMS* + *DC* + *p*-adaptivity indicates the contribution of *p*-adaptivity as well. Positivity is not preserved in the solution obtained with a filter. The sharp front, in fact, makes the filter inappropriate. However, similarly to the steady advection-diffusion test *St-2D*, the VMS-stabilized solution of this problem is characterized as well by the formation of internal layers that run along the edges of the tracer in the direction of the flow (See, e.g., Figure 14b), and VMS is not sufficient to preserve monotonicity unless it is supplemented by the additional *DC* term defined in (27). This effect is displayed in Figures 14,15,16, and 17.

The consideration made for problem *St-2D* on the singular peaks that form at the nodes where the tracer leaves the boundary at an angle, applies here at nodes A and B of Figure 13. This is visible in Figure 18 obtained by slicing the tracer along $z = 0$ in Figures 16 and 17, respectively. The problem is solved by the application of *p*-adaptivity.

As the order of interpolation is increased from 4^{th} to 8^{th}, the smooth solution begins to lose positivity. As interpreted for *St-2D*, the solution is clearly being affected when the interpolation nodes are densely clustered towards the boundaries of the elements, as is the case for higher order.

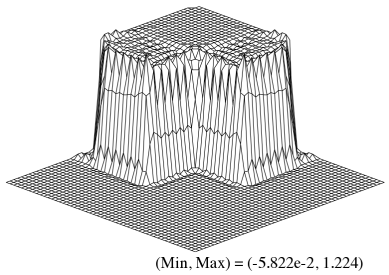

(a) Filter

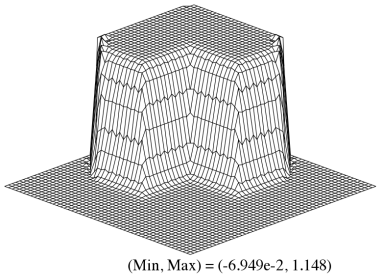

(b) VMS

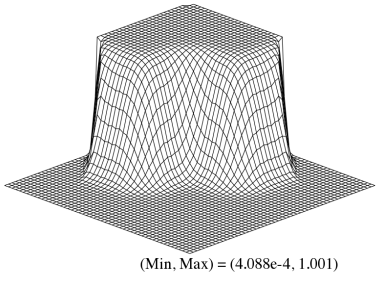

(c) VMS + DC

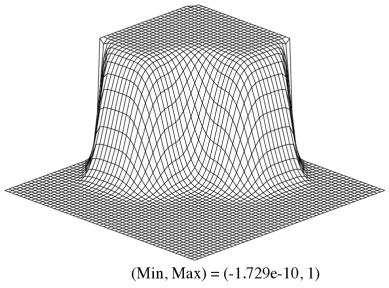

(d) VMS + DC + p-adaptivity

Figure 14: *Tr1-2D*: $4^{th} - order$ 25×25. $t = 0.25\,s$.

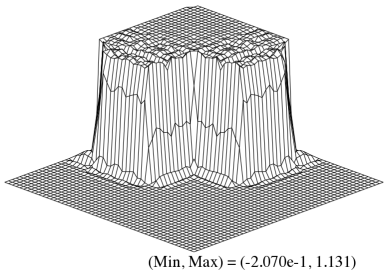

(a) Filter

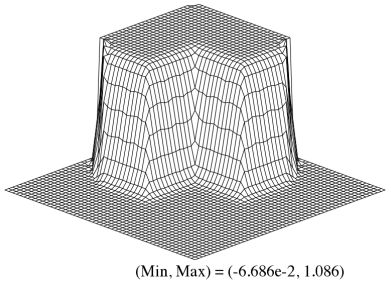

(b) VMS

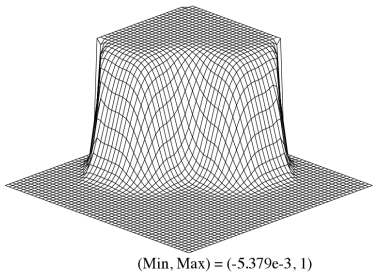

(c) VMS + DC

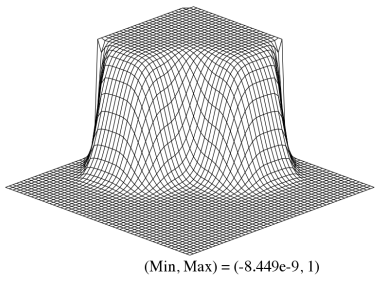

(d) VMS + DC + p-adaptivity

Figure 15: *Tr1-2D*: $8^{th} - order$ 12×12. $t = 0.25\,s$.

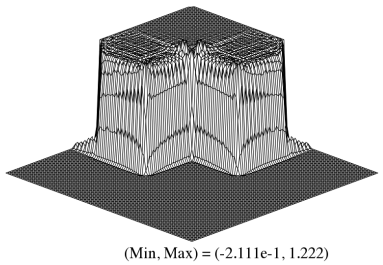

(a) Filter

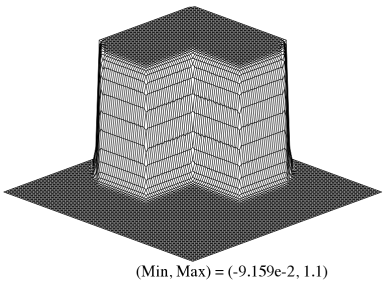

(b) VMS

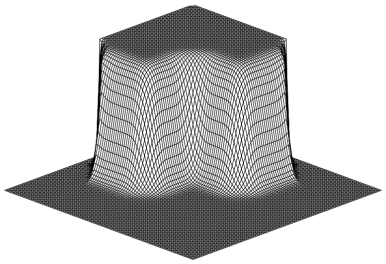

(c) VMS + DC

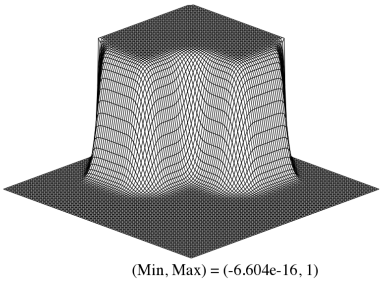

(d) VMS + DC + p-adaptivity

Figure 16: *Tr1-2D*: $4^{th} - order$ 50×50. $t = 0.25\,s$.

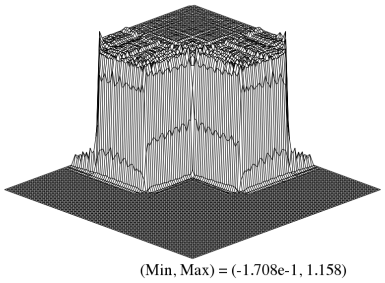

(a) Filter

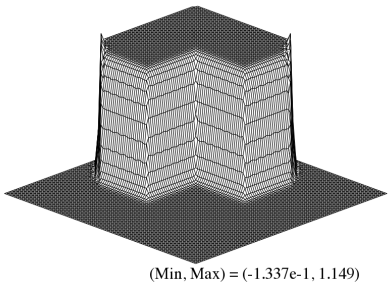

(b) VMS

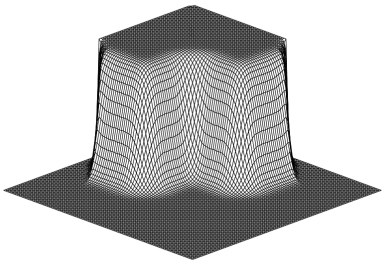

(c) VMS + DC

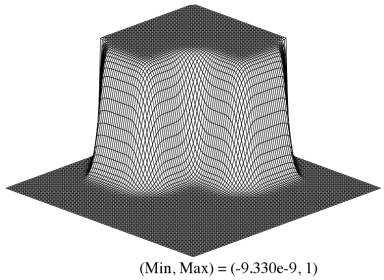

(d) VMS + DC + p-adaptivity

Figure 17: *Tr1-2D*: $8^{th} - order$ 25×25. $t = 0.25\,s$.

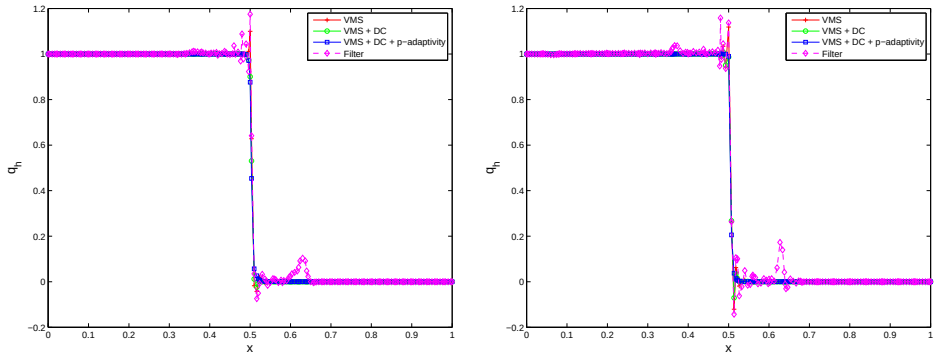

(a) $4^{th} - order$ 50×50 (b) $8^{th} - order$ 25×25

Figure 18: *Tr1-2D*: Vertical slice at $z = 0.0$.

Tr2-2D:. Linear advection of a 2D square wave along x in the periodic domain $\Omega = [0,1] \times [0,1]$: the tracer is transported with velocity $\mathbf{u} = (1/2, 0)\, m\, s^{-1}$ for one periodic revolution along x. The initial concentration $q^h = 1$ is centered at $(x_c, z_c) = (0.5, 0.5)$ (Figure 19). The computational finite domain consists of 11×11 quadrilaterals of order 11.

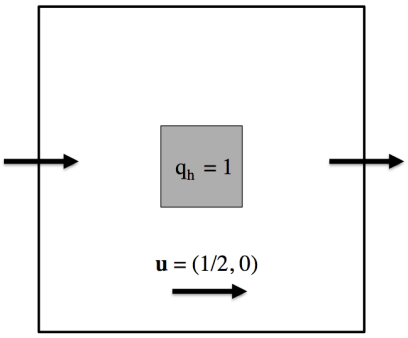

Figure 19: *Tr2-2D*: initial configuration of the pure advection problem.

As in the steady case, Figures 20-22 display improvement of the solution in terms of monotonicity when the VMS method is used instead of the filter. The combination of VMS and filtering is not recommended (result not shown); although VMS alone controls the over- and under-shootings along the streamlines, the addition of the filter at the end of every time step degrades positivity in the neighborhood of large gradients.

In Figures 21 and 22 we present the streamline and crosswind sections of

the solution obtained by slicing the tracer along $z = 0.5$ and $x = 0.5$, respectively. Unlike the previous problems characterized by internal and boundary layers, for pure advection the VMS preserves the maximum and minimum concentrations $q^h_{max} = 1$, and $q^h_{min} = 0$ and is free of spurious oscillations. As a term of comparison, we present the result of classical artificial-viscosity in Figures 20-22*d*. The exact solution of this test at the final time $t = 2$ corresponds to the initial condition. The normalized L_1, L_2 and L_∞ errors of the computed solution with respect to the exact solution were computed on different grids to obtain the convergence curves for different orders of interpolation. Figure 23 shows a log-log plot of the L_∞ error against the grid size $\Delta(x, z) = 0.2, 0.1, 0.05, 0.025, 0.0125, 0.00625$ ($nel = 5 \times 5, ..., 160 \times 160$), where each curve represents the error obtained with different orders of interpolation ($p = 4, ..., 10$). At a given p, the Δt was decreased to maintain a constant Courant number for all resolutions. At a given p, the slope of the curves increases at increasing resolution. This is expected by the spectral element solution in that the error reduces exponentially. However, as p is increased, the slope tends to straighten (See Figure 24), indicating that the larger number of nodes due to the increased p contributes to setting the convergence rate of the method in the same extent as high h-resolution does when p is lower. The data used to generate the plots are reported in Table 2.

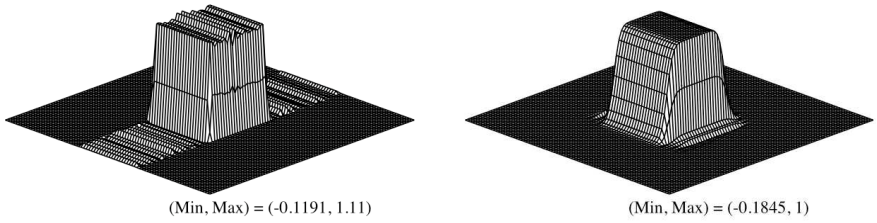

(a) Galerkin (b) Filter

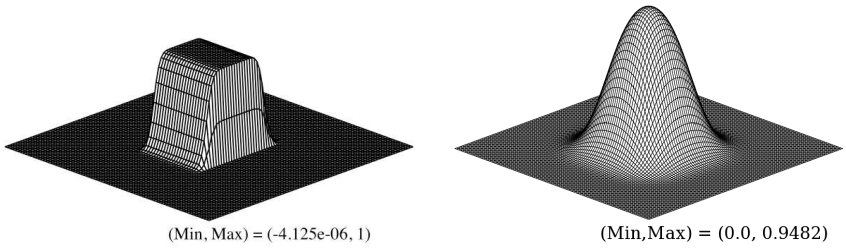

(c) VMS (d) AD/HV $\nu = 0.001\, m^2\, s^{-1}$

Figure 20: *Tr2-2D*: Surface plot of the concentration field: $\Delta t = 0.001\, s$ (except for HV: $\Delta t = 0.0002\, s$), 11×11 elements with 11^{th} order polynomials. Results at t = 2.0 s (after 1 periodic revolution along x).

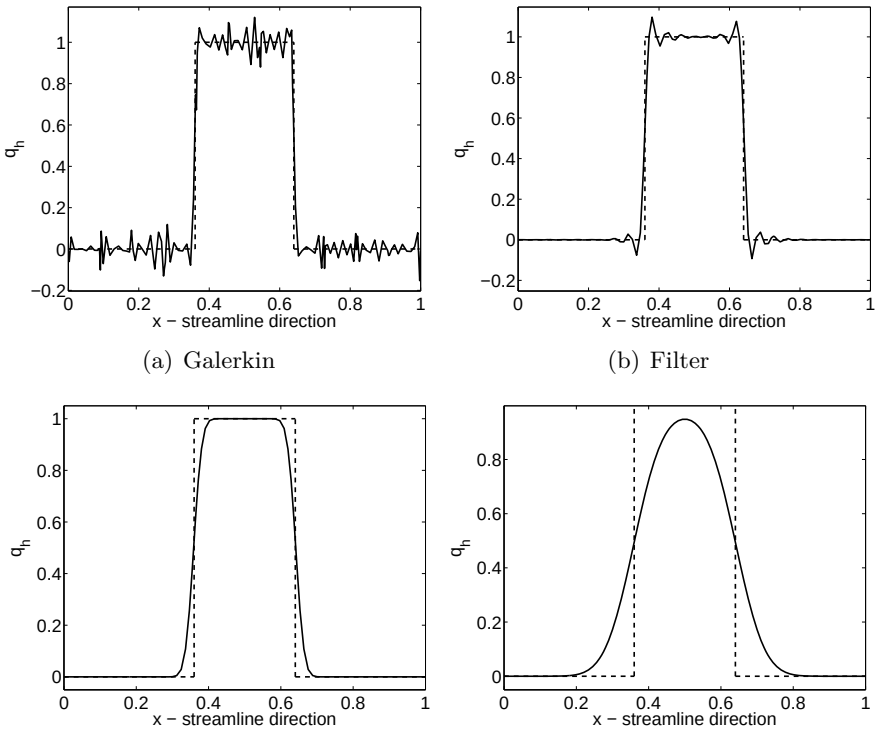

(a) Galerkin (b) Filter

(c) VMS (d) AD/HV $\nu = 0.001\, m^2\, s^{-1}$

Figure 21: *Tr2-2D*: *Streamline* cut at 0.5 m in the y-direction. $\Delta t = 0.001\, s$, 11×11 elements with 11^{th} order polynomials. Results at t = 2 s (after 1 periodic revolution along x). Solid line indicates the computed solution. The dashed line is the analytic solution.

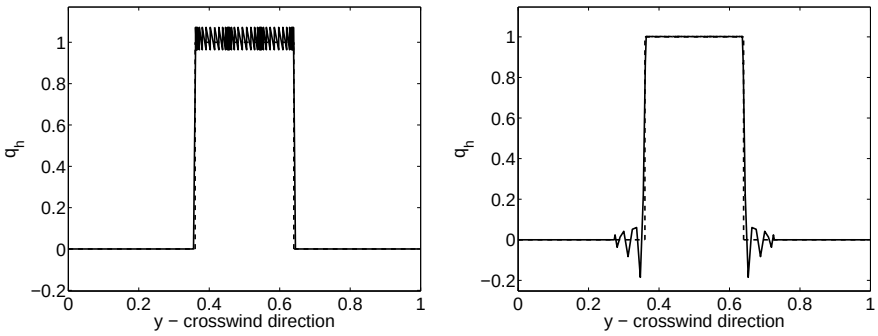

(a) Galerkin

(b) Filter

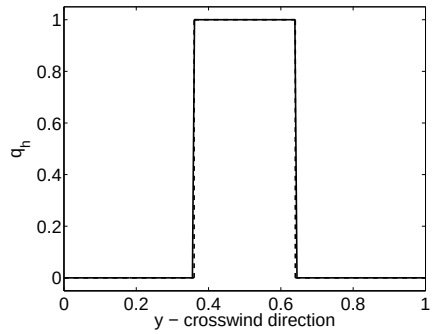

(c) VMS

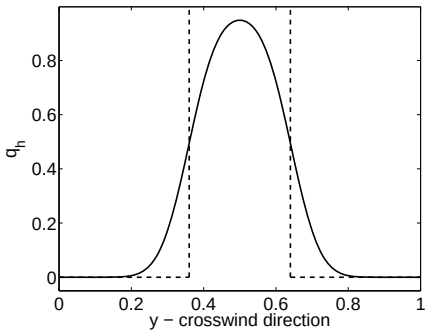

(d) AD/HV $\nu = 0.001\, m^2\, s^{-1}$

Figure 22: *Tr2-2D*: *Crosswind* cut at 0.5 m in the x-direction. $\Delta t = 0.001\, s$, $11{\times}11$ elements with 11^{th} order polynomials. Results at t = 2 s (after 1 periodic revolution along x). Solid line indicates the computed solution. The dashed line is the analytic solution.

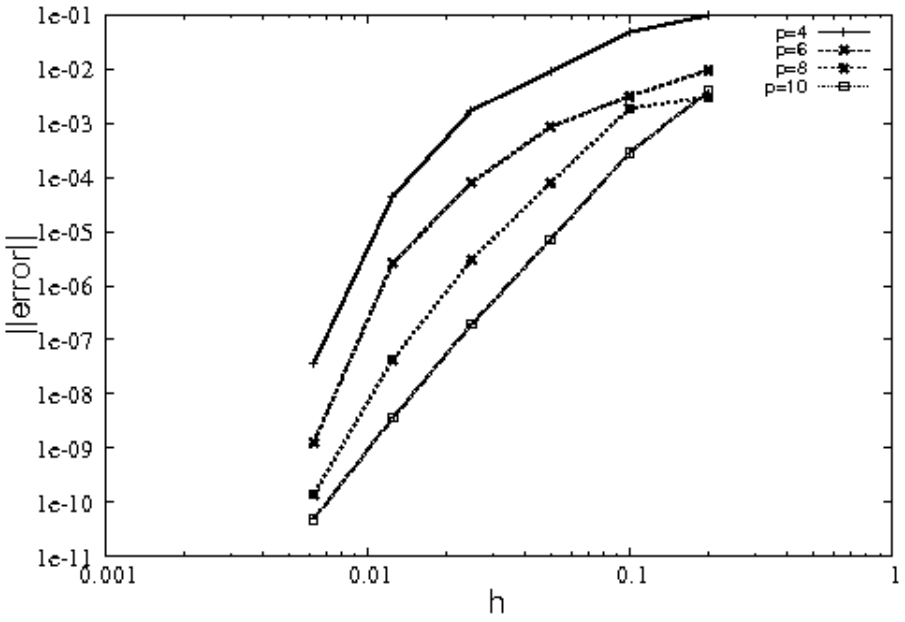

Figure 23: *Tr2-2D*: Log-log plot of the L_∞ norm error *vs.* h for polynomials p *4,6,8,10*. Original tabled data are reported in Appendix B.

Table 2: *Tr2-2D*: Maximum and minimum values of concentration and errors in different norms after 1 full periodic revolution ($t = 2\,s$). $\Delta t = 0.001\,s$, 11×11 elements of 11^{th} order.

Run	q_{min}	q_{max}	L_1	L_2	L_∞	$L_{\infty_{min}}$
FILTER	-0.1951E+00	1.1010	0.13969	0.1732	0.10134E+00	0.10134E+00
VMS	-0.7010E-06	1.0000	0.16581	0.2379	0.10965E-05	0.10965E-05

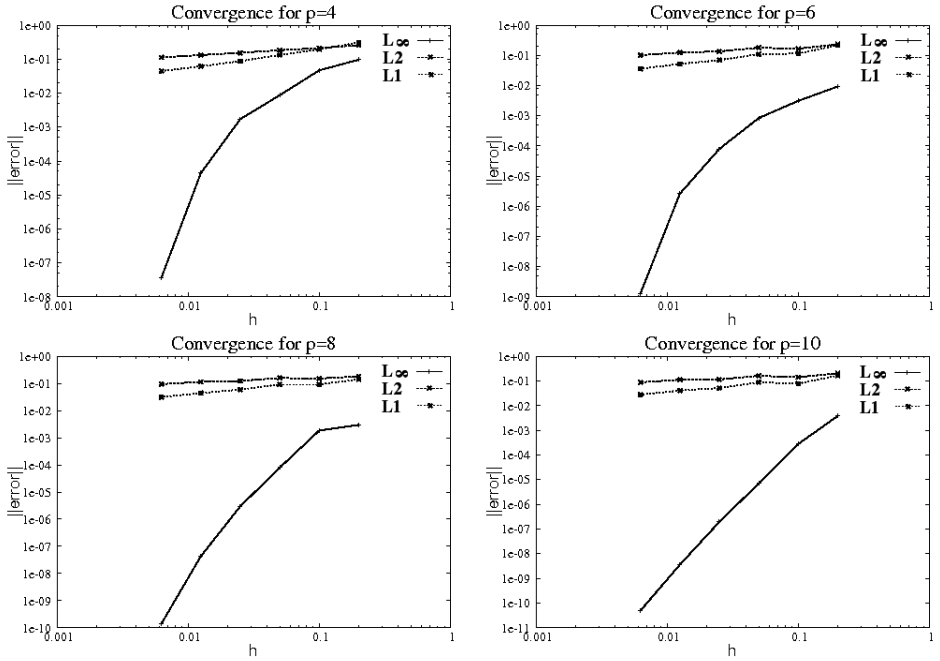

Figure 24: *Tr2-2D*: Log-log plots of the L_1,L_2, and L_∞ norm errors *vs.* h. The original data are reported in Appendix B.

Remark on the use of filters in the previous results: In the current work, filtering was applied in the usual way that has been used previously in SE models (see, e.g., [44, 59, 60, 61]). That is, the filtering coefficients were defined at the beginning of the simulation and applied after every time-step using the same filter matrix for all elements. It may be possible to obtain better results with filters if they are constructed in a specific way (e.g., each element uses a different filter matrix that is constructed dynamically) but a clear approach on how to do this remains an open topic since this can be viewed as a classical limiter but for Spectral Elements (see, e.g., [62]).

5. Discussion and conclusions

5.1. Conclusions

In this paper, we proposed the use of the Variational Multiscale method (VMS) to stabilize advection-dominated problems solved with spectral elements. The stabilization parameter τ that appears in the VMS scheme was computed to include the characteristics of high-order spectral elements with (non-equispaced) LGL nodes. Numerically, we demonstrated that this approach is a possible alternative to the standard filters used in the stabilization of the spectral element solvers if the suppression of unwanted under- and over-shoots is the main concern. In the presence of internal and boundary layers, VMS was coupled with appropriate discontinuity-capturing techniques to damp any oscillations in the proximity of such discontinuities. Stabilization by these methods is obtained by introducing a diffusion-like term that, unlike hyper-viscosity, only acts in the regions where oscillations occur (i.e. large gradients); the solution is not affected in smooth regions. Where needed, the combined action of VMS and polynomial adaptivity yields encouraging results for high-order spectral elements. The algorithms were evaluated on a set of standard tests of increasing difficulty. A significant improvement was observed in the performance of the spectral element solver as far as the control of maxima and minima is concerned, both in the purely advective and in the advective-diffusive regimes. The most important features of this new approach are:

- Unlike hyper-viscosity, the subgrid-scale diffusion only affects regions of the flow where stabilization is required.
- Under- and over-shoots are greatly suppressed relative to traditional filters.
- The method does not depend on a free-parameter assigned by the user.

5.2. Application to atmospheric modeling in climate and weather prediction, and future work

In [63], we implemented a Kessler microphysics scheme [1] within a spectral element framework, that requires the advection of three moisture variables (vapor, cloud, and rain mixing ratios). This microphysics scheme will be implemented in our *Nonhydrostatic Unified Model for the Atmosphere* (NUMA) [64] in order to simulate both mesoscale and synoptic-scale atmospheric phenomena. As is well-known, Galerkin-based methods yield 1) higher-order accuracy and 2) excellent dispersion properties, which are

both desirable for advection schemes; however, the resulting Gibbs oscillations produce strong gradients that must be remedied in some fashion. At present, a simple-minded "fixer" is applied whereby negative values of the moisture variables are set equal to zero. This fixer acts as an effective mass source, thus violating the conservation properties of the model. In addition, this fixer violates the function space that the spectral element solution inhabits. For these reasons, monotonic advection of tracer variables is essential for any atmospheric model. The proposed VMS scheme is an excellent candidate since it 1) preserves monotonicity better than the standard filter approach, 2) does not significantly increase the cost of the spatial discretization scheme, and 3) is completely local in nature (i.e., no additional communications are required in a parallel environment), which is necessary for scaling on modern distributed and hierarchical memory environments. In future work, we will report on the application of VMS to NUMA using realistic mesoscale test cases.

6. Acknowledgements

S.M. and F.X.G. gratefully acknowledge the support of the Office of Naval Research Global (ONRG) that provided support for S.M. through the Visiting Scientist Program through grant N62909-09-1-4083. The work of F.X.G. and J.F.K. was supported by the Office of Naval Research (ONR) through grant PE-0602435N. J.F.K. is supported by the National Research Council (NRC). S.M. and M.V. would like to thank Guillaume Houzeaux and Beatriz Eguzkitza for discussions on the VMS. The remarks of Luca Bonaventura contributed to the improvement of the manuscript. His help is greatly appreciated.

Appendix A. Expression for τ

In this appendix we explicitly derive the expression for τ defined between two consecutive LGL points $[x_{lgl}(i), x_{lgl}(i+1)]$. The bubble obtained from the integration of (17) with boundary conditions $b(x_{lgl}(i)) = 0$ and $b(x_{lgl}(i+1)) = 0$ has expression:

$$b(x) = \frac{x}{u} - \frac{x(i+1) - x(i)}{u(e^{ux(i+1)/\nu} - e^{ux(i)/\nu})} e^{ux/\nu} - \frac{x(i)e^{ux(i+1)/\nu} - x(i+1)e^{ux(i)/\nu}}{u(e^{ux(i+1)/\nu} - e^{ux(i)/\nu})}.$$

The evaluation of the integral (23)

$$\tau_i^{i+1} = \frac{1}{x_{lgl}(i+1) - x_{lgl}(i)} \int_{x_{lgl}(i)}^{x_{lgl}(i+1)} b(x)\, dx$$

yields the expression:

$$\tau_{x(i)}^{x(i+1)} = \frac{1}{x(i+1) - x(i)} \left[\frac{x(i) - x(i+1)}{u} \left(\frac{\nu}{u} + \frac{x(i+1) - x(i)}{2} \right) - \frac{e^{ux(i+1)/\nu} (x(i) - x(i+1))^2}{e^{ux(i)/\nu} - e^{ux(i+1)/\nu}} \right].$$

When $x(i) = 0$ and $x(i+1) = h$, we have that

$$\tau_0^h = -\frac{\nu}{u^2} - \frac{h}{2u} + \frac{h e^{uh/\nu}}{e^{uh/\nu} - 1},$$

from which, after little algebra, expression (20) is recovered:

$$\tau = \frac{h}{2u} \left(\coth(Pe_k) - \frac{1}{Pe_k} \right).$$

Appendix B. Error tables

In this Appendix we report the data of error estimates from which the curves of Figures 23 and 24 were generated.

Table B.3: *Tr2-2D*: Convergence results for the transport problem using the VMS: *p=4*. $\Delta t = 0.001$ for all the runs.

Nelements	L_1	L_2	L_∞	$L_{\infty_{min}}$	q_{max}	q_{min}
5×5	0.30786	0.2583	0.9662E-01	0.1209E+00	1.0970	-0.6290E-01
10×10	0.19662	0.2127	0.4701E-01	0.4770E-01	1.0430	-0.2850E-01
20×20	0.13288	0.1845	0.8739E-02	0.8737E-02	1.0090	-0.6960E-02
40×40	0.87334E-01	0.1546	0.1714E-02	0.1714E-02	1.0020	-0.1793E-02
80×80	0.61619E-01	0.1323	0.4408E-04	0.4408E-04	1.0000	-0.4756E-04
160×160	0.44715E-01	0.1146	0.2650E-07	0.2649E-07	1.0000	-0.4116E-07

Table B.4: *Tr2-2D*: Convergence results for the transport problem using the VMS: *p=4*.
Variable Δt for all the runs: CFL$\simeq$0.01025

Nelements	Δt	L_1	L_2	L_∞	$L_{\infty_{min}}$	q_{max}	q_{min}	M_{loss}
5×5	0.0100E-01	0.3079	0.2583	0.9662E-01	0.1209E+00	1.0970	-0.6290E-01	0.180E-12
10×10	0.0500E-02	0.1966	0.2127	0.4701E-01	0.4770E-01	1.0430	-0.2850E-01	0.182E-12
20×20	0.0250E-02	0.1329	0.1845	0.8739E-02	0.8737E-02	1.0090	-0.6960E-02	0.350E-12
40×40	0.1250E-03	0.8733E-01	0.1546	0.1714E-02	0.1714E-02	1.0020	-0.1793E-02	0.730E-12
80×80	0.6250E-03	0.6162E-01	0.1323	0.4408E-04	0.4408E-04	1.0000	-0.4756E-04	0.147E-11
160×160	0.3125E-04	0.4470E-01	0.1136	0.3661E-07	0.3661E-07	1.0000	-0.5370E-07	0.603E-11

Table B.5: *Tr2-2D*: Convergence results for the transport problem using the VMS: *p=6*.
Variable Δt for all the runs: CFL$\simeq$0.0208

Nelements	Δt	L_1	L_2	L_∞	$L_{\infty_{min}}$	q_{max}	q_{min}	M_{loss}
5×5	0.0100E-01	0.2186	0.2348	0.9349E-02	0.9349E-02	1.0090	-0.8514E-02	0.9084E-12
10×10	0.0500E-02	0.1159	0.1662	0.3126E-02	0.3126E-02	1.0030	-0.2680E-02	0.1810E-11
20×20	0.0250E-02	0.1098	0.1810	0.8451E-03	0.8451E-03	1.0010	-0.5194E-03	0.3642E-11
40×40	0.1250E-03	0.6983E-01	0.1357	0.7971E-04	0.7971E-04	1.0000	-0.9405E-04	0.7241E-11
80×80	0.6250E-03	0.5206E-01	0.1246	0.2599E-05	0.2599E-05	1.0000	-0.2007E-05	0.1454E-10
160×160	0.3125E-04	0.3630E-01	0.1018	0.1276E-08	0.1276E-08	1.0000	-0.1172E-08	0.2904E-10

Table B.6: *Tr2-2D*: Convergence results for the transport problem using the VMS: *p=8*.
Variable Δt for all the runs: CFL$\simeq$0.0352

Nelements	Δt	L_1	L_2	L_∞	$L_{\infty_{min}}$	q_{max}	q_{min}	M_{loss}
5×5	0.0100E-01	0.1415	0.18180	0.2970E-02	0.2970E-02	1.0030	-0.7465E-02	0.9053E-12
10×10	0.0500E-02	0.9237E-01	0.15087	0.1852E-02	0.1852E-02	1.0020	-0.1610E-02	0.1816E-11
20×20	0.0250E-02	0.9162E-01	0.15879	0.7905E-04	0.7905E-04	1.0000	-0.1115E-03	0.3612E-11
40×40	0.1250E-03	0.5929E-01	0.12320	0.2979E-05	0.2979E-05	1.0000	-0.4298E-05	0.7325E-11
80×80	0.6250E-03	0.4432E-01	0.11340	0.4332E-07	0.4332E-07	1.0000	-0.1031E-06	0.1436E-10
160×160	0.3125E-04	0.3129E-01	0.9399E-01	0.1418E-09	0.1418E-09	1.0000	-0.7009E-10	0.2854E-10

Table B.7: *Tr2-2D*: Convergence results for the transport problem using the VMS: *p=10*.
Variable Δt for all the runs: CFL$\simeq$0.0536

Nelements	Δt	L_1	L_2	L_∞	$L_{\infty_{min}}$	q_{max}	q_{min}	M_{loss}
5×5	0.0100E00	0.1647	0.2034	0.3855E-02	0.3855E-02	1.0040	-0.5317E-02	0.9069E-12
10×10	0.0500E-01	0.7786E-01	0.1415	0.2796E-03	0.2796E-04	1.0000	-0.2022E-03	0.1820E-11
20×20	0.0250E-01	0.8875E-01	0.1622	0.7076E-05	0.7076E-05	1.0000	-0.1081E-04	0.3651E-11
40×40	0.1250E-02	0.5183E-01	0.1142	0.1937E-06	0.1937E-06	1.0000	-0.7324E-07	0.7298E-11
80×80	0.6250E-03	0.4083E-01	0.1115	0.3612E-08	0.3612E-08	1.0000	-0.1089E-07	0.1455E-10
160×160	0.3125E-04	0.2785E-01	0.8815E-01	0.4936E-10	0.4936E-10	1.0000	-0.1127E-10	0.2842E-10

References

[1] J. Klemp, R. Wilhelmson, The simulation of three-dimensional convective storm dynamics, J. Atmos. Sci. 35 (1978) 1070–1096.

[2] G. Doms, J. Forstner, E. Heise, H.-J. Herzog, M. Raschendorfer, T. Reinhardt, B. Ritter, R. Schrodin, J.-P. Schulz, G. Vogel, A description of the nonhydrostatic regional model LM. part II: Physical parameterization, Tech. rep., COSMO (2007).

[3] M. Restelli, L. Bonaventura, R. Sacco, A semi-Lagrangian discontinuous Galerkin method for the scalar advection by incompressible flows, J. Comput. Phys. 216 (2006) 195–215.

[4] T. J. R. Hughes, A. N. Brooks, A multidimensional upwind scheme with no crosswind diffusion, in: T. J. R. Hughes (Ed.), Finite element methods for convection dominated flows, ASME, Vol. 32, 1982, pp. 19–35.

[5] P. D. Lax, Accuracy and resolution in the computation of solutions of linear and nonlinear equations, In Recent advances in numerical analysis. Proceeding symposium mathematical research center, Uni. Wisconsin, Academic Press, 1978.

[6] T. Hughes, Multiscale phenomena: Green's functions, the Dirichlet-to-Neumann formulation, subgrid scale models, bubbles and the origins of stabilized methods, Comput. Methods Appl. Mech. and Engrg. 127 (1995) 387–401.

[7] T. J. R. Hughes, G. Feijoo, L. Mazzei, J. Quincy, The variational multiscale method – A paradigm for computational mechanics, Comput. Methods Appl. Mech. Engrg. 166 (1998) 3–24.

[8] C. Johnson, Numerical solution of partial differential equations by the finite element method, Cambridge University Press, 1987.

[9] A. N. Brooks, T. J. R. Hughes, Streamline upwind/Petrov-Galerkin formulations for convective dominated flows with particular emphasis on the incompressible navier-stokes equations, Comput. Methods Appl. Mech. Eng. 32 (1982) 199–259.

[10] T. J. R. Hughes, L. P. Franca, G. M. Hulbert, A new finite element formulation for computational fluid dynamics: VIII. the Galerkin/least-squares method for advective-diffusive equations, Comp. Methods Appl. Mech. Engrg. 73 (1989) 173–189.

[11] C. Johnson, U. Nävert, J. Pitkaranta, Finite element methods for linear hyperbolic problems, Comput. Methods Appl. Mech. Engrg. 45 (1984) 285–312.

[12] U. Nävert, A finite element method for convection-diffusion problems, Ph.D. thesis, Department of Computer Science, Chalmers University of Technology. Goteborg, Sweden (1982).

[13] I. Harari, T. J. R. Hughes, Stabilized finite element methods for steady advection-diffusion with production, Comput. Methods Appl. Mech. Engrg. 115 (1994) 165–191.

[14] L. Franca, C. Farhat, Bubble functions prompt unusual stabilized finite element methods, Comput. Methods Appl. Mech. Engrg. 123 (1995) 299–308.

[15] L. Franca, F. Valentin, On an improved unusual stabilized finite element method for the advective-reactive-diffusive equation, Comput. Methods Appl. Mech. Engrg. 190 (2001) 1785–1800.

[16] F. Pasquarelli, A. Quarteroni, Effective spectral approximations of convection-diffusion equations, Comput. Methods Appl. Mech. Engrg. 116 (1994) 39–51.

[17] C. Canuto, Stabilization of spectral methods by finite element bubble functions, Comp. Methods Appl. Mech. Engrg. 116 (1994) 13–26.

[18] C. Canuto, G. Puppo, Bubble stabilization of spectral Legendre methods for the advection-diffusion equation, Comput. Method Appl. Mech. Engrg. 118 (1994) 239–263.

[19] C. Canuto, V. Van Kemenade, Bubble-stabilized spectral methods for the incomplressible Navier-Stokes equations, Compiut. Methods Appl. Mech. Engrg. 135 (1996) 35–61.

[20] T. J. R. Hughes, J. Stewart, A space-time formulation for multiscale phenomena, J. Comput. Appl. Math. 74 (1996) 217–229.

[21] T. J. R. Hughes, J. A. Cottrell, Y. Bazilevs, Isogeometric analysis: CAD, finite elements, NURBS, exact geometry and mesh refinement, Comput. Methods Appl. Mech. Engrg. 194 (2005) 4135–4195.

[22] S. Godunov, A difference method for numerical calculation of discontinuous solutions of the equations of hydrodynamics, Mat. Sb., translated US Joint Publ. Res. Service, JPRS 7226, 1969 47 (1959) 271–306.

[23] T. J. R. Hughes, M. Mallet, A. Mizukami, A new finite element formulation for computational fluid dynamics: II. beyond SUPG, Comp. Methods Appl. Mech. Engrg. 54 (1986) 341–355.

[24] T. E. Tezduyar, Y. J. Park, Discontinuity-capturing finite element formulations for nonlinear convection-diffusion-reaction equations, Comput. Methods Appl. Mech. and Engrg. 59 (1986) 307–325.

[25] V. John, P. Knobloch, On spurious oscillations at layers diminishing (*sold*) methods for convection-diffusion equations: Part I - *a* review, Comput. Methods Appl. Mech. Engrg. 196 (2007) 2197–2215.

[26] V. John, P. Knobloch, On spurious oscillations at layers diminishing (SOLD) methods for convection-diffusion equations: Part II - analysis for p_1 and q_1 finite elements, Comput. Methods Appl. Mech. Engrg. 197 (2008) 1997–2014.

[27] R. Codina, A discontinuity-capturing crosswind-dissipation for the finite element solution of the convection-diffusion equation, Comput. Methods Appl. Mech. and Engrg. 110 (1993) 325–342.

[28] L. Franca, S. Frey, T. Hughes, Stabilized finite element methods. I: Application to the advective-diffusive model, Comput. Methods Appl. Mech. Eng. 95 (2) (1992) 253–276.

[29] R. Codina, Comparison of some finite element methods for solving the diffusion-convection-reaction equation, Comput. Methods Appl. Mech. Engrg. 156 (1998) 185–210(26).

[30] R. Codina, Stabilization of incompressibility and convection through orthogonal sub-scales in finite element methods, Comput. Methods Appl. Mech. Engrg. 190 (2000) 1579–1599.

[31] R. Codina, E. Oñate, M. Cervera, The intrinsic time for the streamline upwind/Petrov-Galerkin formulation using quadratic elements, Comput. Methods Appl. Mech. Engrg. 94 (1992) 239–262.

[32] F. Shakib, T. J. R. Hughes, Z. Johan, A new finite element formulation for computational fluid dynamics: X. the compressible Euler and Navier-Stokes equations, Comput. Methods Appl. Mech. Engrg. 89 (1991) 141–291.

[33] T. Hughes, G. Sangalli, Variational multiscale analysis: the finie-scale Green's function, projection, optimization, localization, and stabilized methods, SIAM J. Numer. Anal. 45 (2007) 539–557.

[34] G. Houzeaux, B. Eguzkitza, M. Vázquez, A variational multiscale model for the advection-diffusion-reaction equation, Comm. Numer. Meth. Engrg. 25 (2009) 787–809.

[35] G. Hauke, A. García-Olivares, Variational subgrid formulations for the advection-diffusion-reaction equation, Comput. Methods Appl. Mech. Engrg. 190 (2001) 6847–6865.

[36] R. Codina, Stabilized finite element approximation of transient incompressible flows using orthogonal subscales, Comput. Methods Appl. Mech. Engrg. 191 (2002) 4295–4321.

[37] C. Schwab, *p*- and *hp*- Finite Element Methods: Theory and Applications to Solid and Fluid Mechanics, Oxford University Press, 1999.

[38] G. Karniadakis, S. Sherwin, Spectral/hp element methods for CFD, Oxford University Press, London, 1999.

[39] A. Quarteroni, A. Valli, Numerical Approximation of Partial Differential Equations, Springer, 1994.

[40] F. X. Giraldo, The Lagrange-Galerkin spectral element method on unstructured quadrilateral grids, J. Comp. Phys. 147 (1998) 114–146.

[41] R. J. Spiteri, S. J. Ruuth, A new class of optimal high-order strong-stability-preserving time discretization methods, SIAM J. Numer. Anal. 40 (2002) 469–491.

[42] H. Vandeven, Family of spectral filters for discontinuous problems, J. Sci. Comp. 159.

[43] J. P. Boyd, Two comments on filtering for Chebyshev and Legendre spectral and spectral element methods, J. Comp. Phys. 143 (1998) 283–288.

[44] P. F. Fischer, J. S. Mullen, Filter-based stabilization of spectral element methods, Comptes Rendus de lÁcadémie des Sciences - Series I - Mathematics 332 (2001) 265–270.

[45] F. X. Giraldo, Semi-implicit time-integrators for a scalable spectral element atmospheric model, Q. J. R. Meteorol. Soc. 131 (2005) 2431–2454.

[46] J. Douglas, J. Wang, An absolutely stabilized finite element method, Math. Comput. 52 (1989) 495–508.

[47] T. J. R. Hughes, M. Mallet, A new finite element formulation for computational fluid dynamics: III. the generalized streamline operator for multidimensional advective-diffusive systems, Comp. Methods Appl. Mech. Engrg. 58 (1986) 305–328.

[48] T. J. R. Hughes, T. Tezduyar, Finite element methods for first-order hyperbolic systems with particular emphasis pn the compressible Euler equations, Comput. Methods Appl. Mech. Engrg. 45 (1984) 217–284.

[49] L. Franca, S. Frey, Stabilized finite element methods. II: The incompressible Navier-Stokes equations, Comput. Methods Appl. Mech. Eng. 99 (1992) 209–233.

[50] F. Brezzi, M. Bristeau, L. Franca, M. Mallet, G. Rogé, A relationship between stabilized finite element methods and the Galerkin method viwth bubble functions, Comput. Methods Appl. Mech. Engrg. 96 (1992) 117–129.

[51] T. Tezduyar, M. Senga, SUPG finite element computation of inviscid supersonic flows with $yz\beta$ shock-capturing, Computers and Fluids 36 (2007) 147–159.

[52] C. Canuto, A. Russo, V. Van Kemenade, Stabilized spectral methods for the Navier-Stokes equations: Rresidual-free bubbles and preconditioning, Comput. Methods Appl. Mech. Engrg. 166 (1998) 65–83.

[53] F. Brezzi, M. Bristeau, L. Franca, M. Mallet, G. Roge, A relationship between stabilized finite element methods and the Galerkin method with bubble functions, Comput. Methods Appl. Mech. Engrg. 96 (1992) 117–129.

[54] F. Brezzi, L. P. Franca, T. R. Hughes, A. Russo, $b = \int g$, Comput. Meth. Appl. Mech. Eng. 145 (1997) 329 339.

[55] T. J. R. Hughes, M. Mallet, A new finite element formulation for computational fluid dynamics: IV. a discontinuity-capturing operator for multi-dimensional advective-diffusive systems, Comp. Methods Appl. Mech. Engrg. 58 (1986) 329–336.

[56] C. Johnson, A. H. Schatz, L. B. Wahlbin, Crosswind smear and pointwise errors in streamline diffusion finite element methods, Math. Comput. 59 (1987) 25–38.

[57] J. W. Eaton, GNU Octave Manual, Network Theory Limited, 2002.

[58] Y. Bazilevs, V. M. Calo, T. E. Tezduyar, T. J. R. Hughes, YZβ discontinuity capturing for advection-dominated processes with application to arterial drug delivery, Int. J. Numer. Methods Fluids 54 (2007) 593–608.

[59] M. Taylor, J. Tribbia, M. Iskandarani, The spectral element method for the shallow water equations on the sphere, Journal of Computational Physics 130 (1997) 92–108.

[60] F. X. Giraldo, T. Rosmond, A scalable spectral element eulerian atmospheric model (see-am) for numerical weather prediction: Dynamical core tests, Mon. Wea. Rev. 132 (2004) 133–153.

[61] J. Levin, M. Iskandarani, . HaidvogelD, A spectral filtering procedure for eddy-resolving simulations with the spectral element ocean model, J. Comput. Phys. 137 (1997) 130–154.

[62] A. Fournier, M. Taylor, J. Tribbia, The spectral element atmosphere model (seam): High-resolution parallel computation and localized resolution of regional dynamics, Mon. Weath. Rev. 132 (2004) 726–748.

[63] S. Gaberšek, F. X. Giraldo, J. Doyle, Simple dry and moist experiments with a spectral element model, Mon. Wea. Rev. (submitted).

[64] J. F. Kelly, F. X. Giraldo, Development of the nonhydrostatic unified model for the atmosphere (NUMA): limited-area mode, J. Comput. Phys. (submitted).